STAR-RIS and UAV Combination in MEC Networks: Simultaneous Task Offloading and Communications

Han Xiao, *Student Member, IEEE,* Xiaoyan Hu, *Member, IEEE,* Wenjie Wang, *Member, IEEE,* Zhou Su, *Senior Member, IEEE,* Kai-Kit Wong, *Fellow, IEEE*, Kun Yang, *Fellow, IEEE*

***Abstract*—This paper explores a simultaneous tasks offloading and communications (STOC) scheme in mobile edge computing (MEC) networks, supported by the combination of simultaneously transmitting and reflecting reconfigurable intelligent surface (STAR-RIS) and the unmanned aerial vehicle (UAV). Different from the traditional MEC schemes, the proposed scheme concurrently considers the computation and communication capabilities of the MEC networks, which is actually more practical in reality. Specifically, an optimization problem is devised to maximize the weighted sum of the minimum computed task data and communication data, while ensuring the quality of service (QoS) constraints for STOC through joint design of time scheduling, resource allocation, active and passive beamforming, alongside with the UAV trajectory planning. This non-convex problem with strong couplings among variables is challenging to solve directly. Then, a novel alternating optimization method is proposed, leveraging the successive convex approximation (SCA) and semi-definite relaxation (SDR) techniques. We provide sufficient numerical results to validate the effectiveness of the proposed STOC scheme, which demonstrate that the proposed scheme supported by STAR-RIS and UAV outperforms five benchmark schemes in terms of performance gain. It is important to note that the proposed scheme offers a feasible and realistic way for the implementations of STOC in practical MEC networks.**

***Index Terms*—STAR-RIS, unmanned aerial vehicle (UAV), mobile edge computing (MEC), simultaneous tasks offloading and communications (STOC).**

Manuscript received 22 July, 2024; revised 17 December, 2024; accepted 15 January, 2025. The work of Xiaoyan Hu was supported in part by the National Natural Science Foundation of China (NSFC) under Grants 62201449, 62471380, in part by the Young Elite Scientists Sponsorship Program by China Association for Science and Technology (CAST) under Grant No.YESS20230611, in part by the Key R&D Projects of Shaanxi Province under Grant 2023-YBGY-040, in part by the open research fund of National Mobile Communications Research Laboratory, Southeast University (No. 2025D08), in part by the Qin Chuang Yuan High-Level Innovation and Entrepreneurship Talent Program under Grant QCYRCXM-2022-231, and in part by the "Si Yuan Scholar" Foundation. The work of Kun Yang was partly funded by Natural Science Foundation of China (No. 62132004), Jiangsu Major Project on Basic Researches (Grant No.: BK20243059) and Gusu Innovation Project for People (Grant No.: ZXL2024360). This paper has been presented in part at 2024 16th International Conference on Wireless Communications and Signal Processing (WCSP), Hefei, China, October, 2024, DOI: 10.1109/WCSP62071.2024.10827382. The associate editor coordinating the review of this article and approving it for publication was Prof. Le Long. *(Corresponding author: Xiaoyan Hu.)*

H. Xiao, X. Hu, and W. Wang are with the School of Information and Communications Engineering, Xi'an Jiaotong University, Xi'an 710049, China, X. Hu is also with the National Mobile Communications Research Laboratory, Southeast University, Nanjing 210096, China. (email: hanxiaonuli@stu.xjtu.edu.cn, xiaoyanhu@xjtu.edu.cn, wjwang@mail.xjtu.edu.cn).

Z. Su is with the School of Cyber Science and Engineering, Xi'an Jiaotong University, Xi'an 710049, China. (email: zhousu@xjtu.edu.cn).

K.-K. Wong is with the Department of Electronic and Electrical Engineering, University College London, Torrington Place, WC1E 7JE, UK, and also with Yonsei Frontier Lab, Yonsei University, Seoul, Korea. (email: kai-kit.wong@ucl.ac.uk).

K. Yang is with the State Key Laboratory of Novel Software Technology, Nanjing University, Nanjing, 210008, China, and School of Intelligent Software and Engineering, Nanjing University (Suzhou Campus), Suzhou, 215163, China, and School of Computer Science and Electronic Engineering, University of Essex, UK. (email: kyang@ieee.org).

I. Introduction

With the continuous advancement of wireless network technology, there has been a significant increase in the number of Internet of Things (IoT) devices, resulting in a vast amount of requirements for real-time data processing over wireless networks [1]. Additionally, numerous IoT applications require low latency and intensive computational capabilities, such as autonomous driving, augmented & virtual reality, and pervasive gaming, etc. [2]. These applications impose a great challenge for the traditional networks based on centre-cloud computing framework. In order to effectively tackle this challenge, mobile edge computing (MEC) has arisen as a favorable solution by extending the computational capacity from the central cloud to the network edge cloud, which allows efficient data processing in close proximity. Thus, MEC technology has attracted considerable attention from both academic and industry, resulting in various research initiatives aimed at addressing the computation offloading challenges in MEC systems. These efforts primarily focus on reducing latency, conserving energy, and enhancing quality of service (QoS) through resource allocation [3]–[8]. In generally, traditional MEC networks typically place edge servers at predetermined ground locations, e.g., base station (BS) and access point (AP), leading to two primary drawbacks: (i) It is challenging to ensure consistent QoS for users in remote regions or blocked regions. (ii) Terrestrial MEC networks commonly encounter serious signal degradation during data transmission, and thus limit the uplink data offloading performance.

The unmanned aerial vehicle (UAV) technology offers a promising solution to address the aforementioned challenges by leveraging its controllable flexibility in movement. This feature enables the UAV to swiftly navigate to any point in 3D space and increases the probability of establishing a direct line of sight (LoS) with the ground nodes. Therefore, numerous UAV-assisted MEC strategies have been investigated to effectively leverage the benefits offered by UAV [9]–[14]. Although the utilization of UAV has shown great benefits in enhancing computational capabilities of MEC networks, the

current UAV-enabled MEC schemes are normally designed to accommodate uncontrollable wireless propagation environment, leading to significant limitations on task offloading efficiency and ability. To break this performance bottleneck caused by random wireless channels, the technology of reconfigurable intelligent surface (RIS) provides a promising solution [15]. This is because RIS can dynamically modify the electromagnetic characteristics of incoming signals, facilitating the creation of adjustable virtual channels spanning end-to-end. Thus, integrating the RIS and UAV technologies presents a mutually beneficial strategy to enhance the performance gain of MEC networks, given RIS's capacity to modify the wireless propagation environment and the flexibility of UAVs.

A. Related works

Consequently, numerous RIS-assisted UAV-enabled MEC schemes have been investigated and proposed. Some schemes deploy RIS on the surfaces of buildings to assist ground users in offloading signals to UAVs or to facilitate UAVs offloading computational tasks to BSs. Specifically, [16], [17] respectively proposed a RIS-assisted UAV-MEC scheme, where the RIS installed on building is used to improve the task offloading efficiency from users to the MEC server on the UAV. Considering the limited computational capability of the UAV-MEC, the MEC scheme in [18] involves initially transferring computational tasks from ground users to the MEC server located on the UAV serving as the relay. Subsequently, the unprocessed tasks are forwarded to the terrestrial BS by the UAV in the following time slot, aided by the ground RIS. Furthermore, [19] investigates a MEC system that incorporates the cooperation with UAV and RIS, where the RIS is utilized to establish a relay link connecting users to the BS and to improve the relaying capacity of the UAV. Although these MEC schemes can effectively improve the performance gain of the MEC networks, they still exist the following deficiencies: (i) The traditional RIS can only reflect the incoming signals, requiring the transceivers to be located in the same side of RIS, which will significantly limit the coverage of wireless networks and flexibility in deploying RIS. (ii) The UAV plays multiple roles, functioning as MEC platform to handle certain offloaded tasks and relay to transmit remaining tasks to the BS, requiring complex UAV hardware design. (iii) These double-hop MEC strategies rely on the UAV to receive and decode the offloaded tasks and then transmit the unprocessed tasks to the BS, resulting in high energy and time consumption.

To fully exploit the flexibility of UAVs, some studies have proposed the schemes mounting RIS directly on UAVs to facilitate task offloading of users. By leveraging the mobility of UAVs, the airborne RIS can flexibly adjust its position according to practical requirements, thereby optimizing the channel environment and enhancing coverage. In particular, Zhai *et al.* in [20] introduced a MEC framework with a RIS horizontally mounted on UAV. This innovative scheme enables users to divert their computational tasks to terrestrial MEC servers with the reflective capabilities of the RIS. Further in [21], two UAVs and a RIS are adopted, where one UAV loads the RIS to manipulate and reflect the signals containing task information to the MEC server on another UAV which also serves as the relay to offload the remaining computing tasks to the BS. It is worth noting that the proposed aerial RIS-supported MEC schemes can address the shortcoming of the traditional RIS's half-space coverage, since the horizontally placed aerial RIS can reflect all incident signals from the ground users and achieve a 360°-like coverage. However, the conventional RIS is restricted to merely reflecting incoming signals, thereby offering a limited range of options for beamforming the transmitting signals. Consequently, the MEC schemes deploying RIS on the UAV are unable to fully optimize the available computational resources.

Recently, a novel RIS called simultaneous transmitting and reflecting RIS (STAR-RIS) is introduced in [22], [23]. STAR-RIS, as opposed to traditional RIS, is capable of splitting the incoming signal into two parts, with one portion being reflected back in the direction of the incident signal and the other segment being transmitted towards the opposite direction. This functionality enables STAR-RIS to achieve a 360° coverage area, which is twice compared to the traditional RIS. Hence, STAR-RIS possesses enormous application potentials and has been incorporated into various wireless systems, e.g., secure communications systems [24]–[26], integrated sensing and communications (ISAC) systems [27]–[29], and MEC networks [30]–[32]. Specifically, in [32], a novel MEC scheme is suggested, utilizing a STAR-RIS vertically attached to the UAV to manipulate and adjust the tasks offloading signals from users to the MEC server at the ground BS. With the assistance of STAR-RIS's reflection and transmission beamforming capabilities, the ground users distributed in a 360° area can efficiently offload their tasks to the BS. And a large number of simulation results demonstrate that the proposed aerial STAR-RIS-assisted MEC scheme outperforms the baseline schemes including the conventional aerial RIS-supported scheme. However, this scheme also exists the following deficiencies: (i) The stability of vertically installed aerial STAR-RIS is significantly affected by air resistance and wind, especially for STAR-RIS with large size. This will seriously impact the reliability of the systems. (ii) The MEC scheme does not fully leverage the spatial modulation capabilities of the STAR-RIS and it is challenging for this scheme to effectively utilize the computing and communication resources available on the UAV.

B. Motivations and Contributions

Aside from the above shortcomings and challenges faced by UAV-enabled RIS/STAR-RIS assisted MEC schemes, current MEC schemes still lack generality, primarily for the following reasons: (i) Existing MEC schemes are usually designed on the assumption that all users are computation-oriented which only require computational service support. This assumption overlooks the diversity in user requirements, rendering it incomplete for practical networks. (ii) In current 5G and emerging 6G networks, users exhibit distinct service needs. They may engage in computation-intensive and latency-sensitive tasks, such as virtual reality (VR) or augmented reality (AR). Meanwhile, then may also need basic communication-oriented services, such as transmitting voice, text, or video data. Consequently, considering only the computation-oriented services

fails to adequately address the diverse application requirements in practical MEC networks.

Additionally, the MEC networks that can provide both computing and communication services for users may face the following challenges: (i) Except the signal interference among users with similar service demands, it is also necessary to consider the interference among users with different services. Given that the computation-oriented services often transmit larger volumes of task data than the communication-oriented services, the required signal quality varies significantly between services, which introduces additional challenges for interference management. (ii) Considering different demands for computation-oriented and communication-oriented services, balancing task priority and fairness among users becomes a critical challenge taking into account of limited spectrum resources. Thus, developing an effective scheme to manage both computing-centric and communication-centric services is crucial to satisfy various requirements from users, thereby enhancing the overall QoS of the MEC networks.

Tackling the aforementioned challenges provides the main motivations of this paper, where we propose a novel MEC scheme supported by the aerial STAR-RIS attached horizontally on the UAV for the simultaneous task offloading and communications (STOC). To the best of our knowledge, this is the first work on the STOC scheme in MEC networks. The key contributions of this paper are outlined as follows:

- ***The MEC Architecture for STOC with the Combination of UAV and STAR-RIS:*** This study introduces an innovative MEC system for STOC facilitated by the combination of the UAV and STAR-RIS. Distinguished from conventional MEC schemes, the proposed MEC scheme addresses QoS requirements for both computation-oriented and communication-oriented users simultaneously, which is more applicable in real-world situations and offer a practical solution for MEC networks to fulfil STOC. Specifically, the horizontally deployed aerial STAR-RIS can not only mitigate the impact of air resistance and wind during UAV flight, offering a practical solution to tackle the challenges in [32], but also enable users to fully leverage the full-space modulation capabilities of STAR-RIS to offload computation tasks simultaneously to MEC servers on both UAV and BS without requiring the UAV to decode and forward tasks to the BS. Furthermore, users can interact with individuals in different service areas by transmitting their information to the BS with the help of the reflective feature of the STAR-RIS.
- ***Problem Formulation under Practical Constraints:*** To balance the requirements of the computation-oriented and communication-oriented services in the MEC networks, the weighted sum of the minimum offloaded task data and communication data among users are selected as the optimization objective. In order to maximize this objective under QoS constraints, the time scheduling, resource allocation, active and passive beamforming, and the trajectory of the UAV are comprehensively designed. Note that, tackling this formulated optimization problem presents challenges due to the fact that this problem is a max-min optimization problem with strong couplings among optimization variables.
- ***Alternating Algorithm Design with Guaranteed Convergence:*** To address the non-convex optimization issue, an alternating approach is employed wherein the formulated problem is partitioned into four distinct subproblems. In terms of the active beamforming subproblem, the close-form expression can be derived. Regarding the subproblems designing the passive beamforming and UAV trajectory, the semi-definite relaxation (SDR) method and the successive convex approximation (SCA) technique are utilized to transform the subproblems into solvable. It is verified that the convergence of the proposed algorithm can always be guaranteed by the simulation results.
- ***Significant Performance Improvement:*** The efficiency of the proposed MEC scheme for STOC is validated through numerical simulations. With the assistance of the UAV and STAR-RIS, significant performance improvement can be achieved in comparison with five baseline schemes, including the traditional RIS-assisted scheme.

The paper structure is as follows: Section II presents a thorough examination of the system framework for STOC, where the STAR-RIS augmented UAV-powered MEC network is delineated. Section III delves into the optimization problem and iterative algorithm, offering insights into convergence and complexity analysis. In Section IV, the results of numerical simulations are presented to confirm the algorithm and MEC scheme's efficiency. Lastly, Section V concludes the paper.

Notation: Operator $\circ$ signifies the Hadamard product. The operations $(\cdot)^T$, $(\cdot)^H$, and $(\cdot)^{-H}$ denote the transpose, conjugate transpose, and inverse conjugate transpose, correspondingly. $\mathrm{Diag}(\mathbf{a})$ denotes a diagonal matrix whose diagonal elements are composed of the vector $\mathbf{a}$. $\mathrm{diag}(\mathbf{A})$ refers to a vector whose components consist of the diagonal elements of matrix $\mathbf{A}$. Additionally, the symbols $|\cdot|$, $\|\cdot\|$, and $\|\cdot\|_2$ are indicative of the complex modulus, complex vector modulus, and spectral norm, respectively. $\mathbf{I}_M$ denotes the $M \times M$ identity matrix, $\mathbf{E}_{-k}$ is the matrix removed the k-th column of $\mathbf{I}_K$. $\mathrm{eig}\{\mathbf{Y}\}$ denotes the operation of calculating the eigenvalue of matrix $\mathbf{Y}$, $\mathrm{eigvector}\{y\}$ represents the corresponding eigenvector of the eigenvalue y.

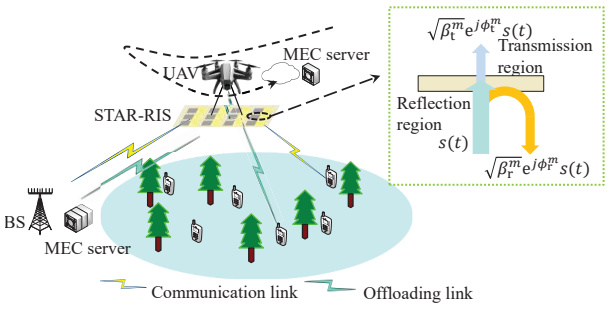

Fig. 1. The multi-user MEC system model for STOC supported by the STAR-RIS and the UAV.

II. System Model

The MEC system model for STOC assisted by STAR-RIS and UAV is illustrated in Fig. 1[1], which comprises K single-antenna users, a N_{t}-antenna BS equipped with a powerful MEC server, a UAV outfitted with a MEC server and a horizontally placed STAR-RIS with M-element [2]. The energy splitting protocol is implemented for STAR-RIS, which demonstrates that all components integrated within the STAR-RIS are able to reflect (R mode) and transmit (T mode) incoming signals concurrently [22]. It is assumed that the direct links between the BS and users are posited to be obstructed by physical barriers like buildings and trees.

It is important to note that each user has two kinds of service requirements, which include the computing-oriented service and the communication-oriented service. For the computing-oriented service, the users are allowed to simultaneously delegate their tasks to the MEC servers positioned at the BS and UAV through the aid of the STAR-RIS's R&T mode, which is beneficial for users to conserve energy and efficiently handle computation-intensive and delay-sensitive tasks. On the other hand, the communication-oriented service entails users establishing uplink communications with the BS for traditional information transmissions. It is generally assumed that the two services cannot be executed concurrently due to the constraint of each user having only one antenna.

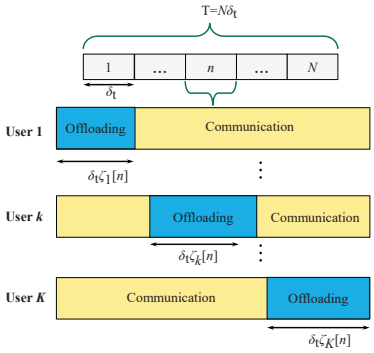

Fig. 2. TDMA-based structure for task offloading.

Given the fact that the UAV is equipped with a single-antenna, we leverage the time division multiple access (TDMA) protocol for users to deal with the computing-oriented service so as to efficiently distribute and manage the offloaded tasks. Specifically, the duration of the mission, denoted by T, is divided into N equal time intervals represented by $\delta_{\mathrm{t}} = \frac{T}{N}$. These intervals are sufficiently small, ensuring that the UAV's position can be considered constant throughout each time slot δ_{t}. Each time slot is further subdivided into K sub-slots designated for individual users to delegate their computational workloads, as depicted in Fig. 2. The duration of each sub-slot is denoted by $\delta_{\mathrm{t}}\zeta_k[n]$, where the variable $\zeta_k[n] \in [0,1], \mathcal{K} \triangleq \{1, \cdots, K\}$ is responsible for determining the amount of time allotted to the k-th user for task offloading within a given time slot, which is constrained as

$$\sum_{k=1}^{K} \zeta_k[n] = 1, \ \forall n \in \mathcal{N} \triangleq \{1, \cdots, N\}, \tag{1}$$

$$0 \leq \zeta_k[n] \leq 1, \ \forall k \in \mathcal{K}, n \in \mathcal{N}. \tag{2}$$

It is easy to note that only one user at maximum is offloading computing tasks to the MEC servers at any time due to the use of the TDMA protocol for task offloading. Except the offloading time for user k in each time slot, it is assumed that user k can leverage the remaining time, i.e., $\delta_{\mathrm{t}}\left(1-\zeta_k[n]\right)$, to enjoy the communication-oriented service for transmitting information to the BS. In other words, except the offloading user, the other $K-1$ users can simultaneously transmit information signals to the BS. In this way, we can efficiently satisfy the requirements of the co-existing computing-oriented and communications-oriented users in the MEC system.

Remark 1. *Actually, the task offloading signal transmitted by the chosen computing-oriented user and the communication signals generated by the $(K-1)$ communications-oriented users will mutually disrupt each other, leading to a decline in both the communication quality and computing power of the MEC network under consideration. The task offloading signal received by the UAV is susceptible to significant interference. This is because the UAV, which is equipped with a single antenna, lacks the capability to mitigate the interference caused by $(K-1)$ communication signals. Instead, it relies solely on the transmitted coefficient of the STAR-RIS to improve the signal-to-interference-plus-noise-ratio (SINR) of the task offloading signal at the UAV.*

Therefore, to ensure that users are able to obtain the high quality experience in both services, it is imperative to strike a balance through the strategic planning of the UAV's trajectory, the implementation of passive and active beamforming techniques, as well as efficient allocation of resources.

To clearly specify the positions of all system nodes, it is assumed that all points are located in a 3D Cartesian coordinate system. The coordinates of the BS and the k-th user are represented as $\mathbf{q}_{\mathrm{BS}} = [x_{\mathrm{BS}}, y_{\mathrm{BS}}, z_{\mathrm{BS}}]^T$ and $\mathbf{q}_k = [x_k, y_k, 0]^T$ respectively, with z_{BS} denoting the vertical position of the BS. Furthermore, it is considered that the UAV operates at a fixed altitude H and maintains a constant position during a time slot. Thus, the UAV's location in the n-th time slot is denoted by $\mathbf{q}_{\mathrm{ua}}[n] = [x_{\mathrm{ua}}[n], y_{\mathrm{ua}}[n], H]^T$ for $n \in \mathcal{N}$, subject to specific flying constraints.

$$\mathbf{v}_{\mathrm{ua}}[n] = \frac{\mathbf{q}_{\mathrm{ua}}[n] - \mathbf{q}_{\mathrm{ua}}[n-1]}{\delta_{\mathrm{t}}}, \|\mathbf{v}_{\mathrm{ua}}[n]\| \leq v_{\max}, \forall n \in \mathcal{N}, \tag{3}$$

$$\mathbf{a}_{\mathrm{ua}}[n] = \frac{\mathbf{v}_{\mathrm{ua}}[n] - \mathbf{v}_{\mathrm{ua}}[n-1]}{\delta_{\mathrm{t}}}, \|\mathbf{a}_{\mathrm{ua}}[n]\| \leq a_{\max}, \forall n \in \mathcal{N}, \tag{4}$$

$$\mathbf{q}_{\mathrm{ua}}[0] = \mathbf{q}_{\mathrm{I}}, \ \mathbf{q}_{\mathrm{ua}}[N] = \mathbf{q}_{\mathrm{F}}, \tag{5}$$

[1]Note that the RIS system consists of lightweight composite substrate materials, ultra-thin metallic layers, and simple control circuitry, making it inherently lightweight and able to manipulate incident signals with simple hardware, resulting in very low additional energy consumption for UAVs.

[2]While the horizontally placed aerial STAR-RIS can effectively reduce the impact of wind on its stability, this approach still has certain limitations. To further mitigate the effects of wind on the aerial RIS, it is worth considering the integration of the following solutions in the future work: (i) Exploring the electromagnetic characteristic of RIS to design more miniatured RIS systems. (ii) Establishing a jitter model specifically for the aerial RIS and designing the highly robust aerial RIS-assisted communication schemes.

where $\|\mathbf{v}_{\rm ua}[n]\|$ and $\|\mathbf{a}_{\rm ua}[n]\|$ respectively denote the flying velocity and acceleration of the UAV, and $v_{\max}$ and $a_{\max}$ are the corresponding maximum values. $\mathbf{q}_{\rm I}$ and $\mathbf{q}_{\rm F}$ are the initial and final positions of the UAV trajectory which can be treated as the ground stations for UAV, providing dependable power supply and facilitating required maintenance.

A. Channel Model

In this paper, the STAR-RIS is considered to be a uniform planar array (UPA) comprising M_x elements in the x-axis orientation and M_y elements in the y-axis orientation, with the total number of elements represented as $M = M_x M_y$. The communication channels between the UAV and the users are primarily influenced by the Rician channel. Therefore, the channel corresponding to user k during the n-th time slot is represented as $\mathbf{h}_{{\rm u}k}[n]$, which is given by

$$\mathbf{h}_{{\rm u}k}[n] = \sqrt{\frac{\rho}{d_{{\rm u}k}^{\alpha_{{\rm u}k}}[n]}}\widehat{\mathbf{h}}_{{\rm u}k}[n] \in \mathbb{C}^{M\times 1}, \tag{6}$$

where $\rho = (\frac{\lambda}{4\pi})^2$ denotes the path loss occurring at a standardized distance of 1 meter, where λ signifies the wavelength linked to the carrier frequency under consideration. $d_{{\rm u}k}$ denotes the distance between the UAV and the k-th user, $\alpha_{{\rm u}k}$ is the path-loss exponent value. $\widehat{\mathbf{h}}_{{\rm u}k}[n] = \sqrt{\frac{\beta}{1+\beta}}\mathbf{h}_{{\rm u}k}^{\rm LOS}[n] + \sqrt{\frac{1}{1+\beta}}\mathbf{h}_{{\rm u}k}^{\rm NLOS}[n]$ is the Rician fading with β being the Rician factor. $\mathbf{h}_{{\rm u}k}^{\rm NLOS}[n] \sim \mathcal{CN}(0, \mathbf{I}_M)$ denotes the non line-of-sight (NLoS) component, and $\mathbf{h}_{{\rm u}k}^{\rm LOS}[n]$ is the LoS component, which is expressed as

$$\begin{aligned}&\mathbf{h}_{{\rm u}k}^{\rm LOS}[n] = \\ &\left[1, \cdots, e^{-j\frac{2\pi d}{\lambda}(m_{\rm x}-1)\xi_{{\rm u}k}[n]}, \cdots, e^{-j\frac{2\pi d}{\lambda}(M_{\rm x}-1)\xi_{{\rm u}k}[n]}\right]^T \otimes \\ &\left[1, \cdots, e^{-j\frac{2\pi d}{\lambda}(m_{\rm y}-1)\chi_{{\rm u}k}[n]}, \cdots, e^{-j\frac{2\pi d}{\lambda}(M_{\rm y}-1)\chi_{{\rm u}k}[n]}\right]^T,\end{aligned} \tag{7}$$

where $\xi_{{\rm u}k}[n] = \cos(\phi_{{\rm u}k}[n])\sin(\theta_{{\rm u}k}[n]) = \frac{x_{\rm ua}-x_k}{\|\mathbf{q}_{\rm ua}[n]-\mathbf{q}_k\|}$ and $\chi_{{\rm u}k}[n] = \sin(\phi_{{\rm u}k}[n])\sin(\theta_{{\rm u}k}[n]) = \frac{y_{\rm ua}-y_k}{\|\mathbf{q}_{\rm ua}[n]-\mathbf{q}_k\|}$, with $\phi_{{\rm u}k}[n]$ and $\theta_{{\rm u}k}[n]$ representing the azimuth and elevation angles of arrival (AoA) for signals from user k to the STAR-RIS.

It is assumed that the BS adopts the uniform linear array (ULA) with $N_{\rm t}$ antennas. Given that the BS remains stationary at a fixed position and has an altitude denoted as $z_{\rm BS}$, the LoS channel model is utilized to describe the connection between the BS and the UAV. This connection $\mathbf{H}_{\rm BR}[n] \in \mathbb{C}^{M\times N_{\rm t}}$ at the n-th time slot is represented by the following expression:

$$\mathbf{H}_{\rm BR}[n] = \sqrt{\frac{\rho}{d_{\rm BR}^{\alpha_{\rm BR}}[n]}}\widehat{\mathbf{H}}_{\rm BR} = \sqrt{\frac{\rho}{d_{\rm BR}^{\alpha_{\rm BR}}[n]}}\mathbf{a}_{\rm R}^{\rm BR}[n]\mathbf{a}_{\rm B}^H[n], \tag{8}$$

where $\mathbf{a}_{\rm R}^{\rm BR}[n]$ and $\mathbf{a}_{\rm B}[n]$ respectively represent the beam steering vectors of the UPA and ULA at the STAR-RIS and the BS, which are given by

$$\begin{aligned}&\mathbf{a}_{\rm R}^{\rm BR}[n] = \\ &\left[1, \cdots, e^{-j\frac{2\pi d}{\lambda}(m_{\rm x}-1)\xi_{\rm BR}[n]}, \cdots, e^{-j\frac{2\pi d}{\lambda}(M_{\rm x}-1)\xi_{\rm BR}[n]}\right]^T \otimes \\ &\left[1, \cdots, e^{-j\frac{2\pi d}{\lambda}(m_{\rm y}-1)\chi_{\rm BR}[n]}, \cdots, e^{-j\frac{2\pi d}{\lambda}(M_{\rm y}-1)\chi_{\rm BR}[n]}\right]^T,\end{aligned} \tag{9}$$

$$\begin{aligned}&\mathbf{a}_{\rm B}[n] = \\ &\left[1, \cdots, e^{-j\frac{2\pi d}{\lambda}(n_{\rm t}-1)\gamma[n]}, \cdots, e^{-j\frac{2\pi d}{\lambda}(N_{\rm t}-1)\gamma[n]}\right]^T,\end{aligned} \tag{10}$$

where $\xi_{\rm BR}[n] = \cos(\phi_{\rm BR}[n])\sin(\theta_{\rm BR}[n]) = \frac{x_{\rm BS}-x_{\rm ua}[n]}{\|\mathbf{q}_{\rm BS}[n]-\mathbf{q}_{\rm ua}\|}$ and $\chi_{\rm BR}[n] = \sin(\phi_{\rm BR}[n])\sin(\theta_{\rm BR}[n]) = \frac{y_{\rm BS}-y_{\rm ua}[n]}{\|\mathbf{q}_{\rm BS}[n]-\mathbf{q}_{\rm ua}\|}$ with $\phi_{\rm BR}[n]$ and $\theta_{\rm BR}[n]$ representing the azimuth and elevation angles of departure (AoD) for signals from the STAR-RIS to the BS. In addition, $\gamma[n] = \frac{\sqrt{(y_{\rm BR}-y_{\rm ua})^2+(x_{\rm BR}-x_{\rm ua})^2}}{\|\mathbf{q}_{\rm BR}-\mathbf{q}_{\rm ua}[n]\|}$.

Due to the close proximity between the UAV and the STAR-RIS, the near-field channel is utilized to represent the association between the UAV and the STAR-RIS taking into account the electromagnetic fields' spherical wave properties. This near-field channel, denoted as $\mathbf{h}_{\rm ru}$, is given by [33].

$$\mathbf{h}_{\rm ru} = \boldsymbol{\alpha} \circ \mathbf{a}_{\rm ru} \in \mathbb{C}^{M\times 1}, \tag{11}$$

where we have

- $\boldsymbol{\alpha} = \left[\frac{\lambda}{4\pi r_1}, \cdots, \frac{\lambda}{4\pi r_m}, \cdots, \frac{\lambda}{4\pi r_M}\right]^T$,
- $\mathbf{a}_{\rm ru} = \left[e^{-j\frac{2\pi r_1}{\lambda}}, \cdots, e^{-j\frac{2\pi r_m}{\lambda}}, \cdots, e^{-j\frac{2\pi r_M}{\lambda}}\right]^T$.

Here, r_m is the distance between UAV's antenna and the m-th element of the STAR-RIS, $\forall m \in \mathcal{M} \triangleq \{1, \cdots, M\}$. The unchanging nature of the channel $\mathbf{h}_{\rm ru}$ can be deduced from the consistent spatial relationship observed between the antenna of the UAV and the elements of the STAR-RIS.

B. Computation Model

According to the above analysis, when the k-th user is selected to offload its computing tasks to MEC servers with the allocated time $\delta_{\rm t}\zeta_k[n]$ in n-th time slot, the SINR at the BS and the UAV can respectively expressed as

- $\gamma_k^{\rm BS}[n] = \dfrac{p_{\rm u}\left|\mathbf{w}_k^H[n]\mathbf{H}_{\rm BR}^H[n]\mathbf{U}_{\rm r}^H[n]\mathbf{h}_{{\rm u}k}[n]\right|^2}{\underbrace{p_{\rm u}\sum\limits_{j\neq k}^{K}\left|\mathbf{w}_k^H[n]\mathbf{H}_{\rm BR}^H[n]\mathbf{U}_{\rm r}^H[n]\mathbf{h}_{{\rm u}j}[n]\right|^2}_{\text{Communication Interference}} + \sigma_{\rm BS}^2\mathbf{w}_k^H[n]\mathbf{w}_k[n]}$,
- $\gamma_k^{\rm ua}[n] = \dfrac{p_{\rm u}\left|\mathbf{h}_{\rm ru}^H\mathbf{U}_{\rm t}[n]\mathbf{h}_{{\rm u}k}[n]\right|^2}{\underbrace{p_{\rm u}\sum\limits_{j\neq k}^{K}\left|\mathbf{h}_{\rm ru}^H\mathbf{U}_{\rm t}[n]\mathbf{h}_{{\rm u}j}[n]\right|^2}_{\text{Communication Interference}} + \sigma_{\rm u}^2}$,

where $p_{\rm u}$ is the unified transmitting power of all users. In addition, $\mathbf{U}_\varepsilon[n] = {\rm Diag}\{\sqrt{\beta_\varepsilon^1[n]}e^{j\phi_\varepsilon^1[n]}, \cdots, \sqrt{\beta_\varepsilon^m[n]}e^{j\phi_\varepsilon^m[n]}, \cdots, \sqrt{\beta_\varepsilon^M[n]}e^{j\phi_\varepsilon^M[n]}\}$ with $\varepsilon \in \{{\rm r}, {\rm t}\}$ respectively represent the reflection and transmission coefficient matrices for STAR-RIS, where the amplitude and phase of the STAR-RIS need to satisfy the constraints: $\beta_{\rm r}^m[n] + \beta_{\rm t}^m[n] = 1$, $\phi_\varepsilon^m[n] \in [0, 2\pi)$, $\forall m \in \mathcal{M}, n \in \mathcal{N}$. $\mathbf{w}_k[n] \in \mathbb{C}^{N\times 1}$ is the received beamforming vector at the BS for user k in time slot n. $\sigma_{\rm BS}^2$ and $\sigma_{\rm u}^2$ are the noise power at the BS and the UAV, respectively. It is worth noting that the signal for task offloading from the k-th user at the BS experiences interference from the communication signals of the $(K-1)$ remaining users.

It is important to highlight that the offloading signal is only interfered by the communication signals of other users as a result of employing the TDMA protocol in the process of task offloading. Hence, the achievable task offloading rates for user

k to the MEC servers at the BS and UAV in the n-th time slot can be respectively expressed as

$$R_k^{\mathrm{BS}}[n] = B\log_2\left(1+\gamma_k^{\mathrm{BS}}[n]\right), \tag{12}$$

$$R_k^{\mathrm{ua}}[n] = B\log_2\left(1+\gamma_k^{\mathrm{ua}}[n]\right), \tag{13}$$

where B is the available bandwidth of the considered system.

In this paper, it is presumed that users refrain from employing local computing for tasks given the constraints of limited resources and the objective of energy conservation. Thus, users are required to transfer their computational workloads to MEC servers positioned at the BS and UAV. $l_k^{\mathrm{BS}}[n]$ and $l_k^{\mathrm{ua}}[n]$ denote the data volume requiring processing at the BS and the UAV respectively, for user k during the n-th time slot. Taking into account the restrictions on achievable offloading rates, the information-causality constraints are as follows.

- $\delta_{\mathrm{t}}\zeta_k[n]R_k^{\mathrm{BS}}[n] \geq l_k^{\mathrm{BS}}[n],\ \forall k\in\mathcal{K}, n\in\mathcal{N}$,
- $\delta_{\mathrm{t}}\zeta_k[n]R_k^{\mathrm{ua}}[n] \geq l_k^{\mathrm{ua}}[n],\ \forall k\in\mathcal{K}, n\in\mathcal{N}$.

The frequencies designated by the BS and the UAV for handling the tasks of the k-th user during the n-th time slot are respectively represented as $f_k^{\mathrm{BS}}[n]$ and $f_k^{\mathrm{ua}}[n]$. It is essential to ensure the proper sequencing of task processing. We assume that both the BS and the UAV will solely receive the transferred tasks in the first time slot without carrying out any calculations. Furthermore, it is assumed that users will stop offloading their tasks in the final time slot, i.e., $f_k^{\mathrm{ua}}[1] = l_k^{\mathrm{ua}}[N] = f_k^{\mathrm{BS}}[1] = l_k^{\mathrm{BS}}[N] = 0$. The following information-causality constraints are in place to guarantee that the tasks delegated by K users can be fully processed within the designated mission period T, which is given by

$$\sum_{k=1}^{K} f_k^{\mathrm{BS}}[n] \leq F_{\mathrm{BS}},\ \sum_{k=1}^{K} f_k^{\mathrm{ua}}[n] \leq F_{\mathrm{ua}},\ \forall n\in\mathcal{N}, \tag{14}$$

$$\sum_{i=2}^{n}\frac{f_k^{\mathrm{ua}}[i]\delta_{\mathrm{t}}}{\varrho_{\mathrm{ua}}} \geq \sum_{i=1}^{n-1} l_k^{\mathrm{ua}}[i],\ n\in\mathcal{N}_1, \tag{15}$$

$$\sum_{i=2}^{n}\frac{f_k^{\mathrm{BS}}[i]\delta_{\mathrm{t}}}{\varrho_{\mathrm{BS}}} \geq \sum_{i=1}^{n-1} l_k^{\mathrm{BS}}[i],\ n\in\mathcal{N}_1, \tag{16}$$

where F_{BS} and F_{ua} are the maximum CPU frequency offered by the BS and the UAV, respectively. ϱ_{BS} and ϱ_{ua} denote the CPU cycles required to process 1-bit data at the BS and the UAV, respectively. $\mathcal{N}_1 \triangleq \{2,3,\cdots,N\}$ is a sub-set of $\mathcal{N}$.

Furthermore, let $l_{\min}^{\mathrm{o}}$ denotes the smallest number of tasks that should be offloaded by users throughout the entire mission duration T. This minimum offloading requirement metric is crucial in assessing the system's computational capacity to process computing tasks effectively while maintaining fairness and equitable distribution among all users. Moreover, to guarantee that each user's minimum computational requirement is satisfied, the following QoS constraint is considered:

- $l_{\min}^{\mathrm{o}} = \min_{k\in\mathcal{K}}\left(\sum_{n=1}^{N} l_k^{\mathrm{BS}}[n] + l_k^{\mathrm{ua}}[n]\right) \geq L_{\mathrm{o}}$,

where L_{o} denotes the minimum computing tasks that each user needs to offload.

C. Communication Model

Recall that each user requires the aerial platform assisted by the STAR-RIS and the UAV to provide two services for them within a given time slot, i.e., the computing-oriented service and the communication-oriented service. In particular, when the k-th user communicates with the BS, the SINR of the received signal for k-th user at the BS can be expressed as

- $$\tilde{\gamma}_k^{\mathrm{BS}}[n] = \frac{p_{\mathrm{u}}\left|\mathbf{w}_k^H[n]\mathbf{H}_{\mathrm{BR}}^H[n]\mathbf{U}_{\mathrm{r}}^H[n]\mathbf{h}_{\mathrm{u}k}[n]\right|^2}{\underbrace{p_{\mathrm{u}}\sum_{j\neq k}^{K}\left|\mathbf{w}_k^H[n]\mathbf{H}_{\mathrm{BR}}^H[n]\mathbf{U}_{\mathrm{r}}^H[n]\mathbf{h}_{\mathrm{u}j}[n]\right|^2}_{\text{Communication and Offloading Interference}} + \sigma_{\mathrm{BS}}^2\mathbf{w}_k^H[n]\mathbf{w}_k[n]}.$$

Remark 2. The k-th user's communication signal is interfered by the $(K-2)$ communication signals and one task offloading signal. Considering that the quasi-static channels between the STAR-RIS and users/BS are unchanged within a time slot due to each time slot is sufficient small, the same active beamforming vectors, as well as reflection and transmission coefficients of the STAR-RIS are employed to support all user's transmission of both computing and communication data in the given time slot. This explains why the expressions for $\gamma_k^{BS}[n]$ and $\tilde{\gamma}_k^{BS}[n]$ are identical. However, from the perspective of signal types of interest and interfering signal composition, $\tilde{\gamma}_k^{\mathrm{BS}}[n]$ and $\gamma_k^{\mathrm{BS}}[n]$ carry distinct meanings. Hence, we utilize two symbols to represent them separately. Additionally, due to the same expression of $\gamma_k^{BS}[n]$ and $\tilde{\gamma}_k^{BS}[n]$, we can leverage the rate $R_k^{\mathrm{BS}}[n]$ to represent the communication rate of the k-th user in the n-th time slot.

Let $l_{\min}^{\mathrm{c}}$ denotes the minimum amount of communication data that are transmitted by users during the whole mission period T, which is expressed as

- $l_{\min}^{\mathrm{c}} = \min_{k\in\mathcal{K}}\sum_{n=1}^{N}\delta_{\mathrm{t}}(1-\zeta_k[n])R_k^{\mathrm{BS}}[n]$.

Note that $l_{\min}^{\mathrm{c}}$ is an important performance indicator to measure the communication capability of the considered MEC network taking the fairness among all users into account. To guarantee that each user's minimum communication requirement is satisfied, the communication QoS constraint $l_{\min}^{\mathrm{c}} \geq L_{\mathrm{c}}$ will be considered, where L_{c} is the minimum amount of communication data required by each user.

III. Problem Formulation and Algorithm Design

A. Problem Formulation

The section will present the optimization problem based on the analysis outlined in Section II. The objective is to maximize the weighted sum of the minimum offloaded tasks, denoted as $l_{\min}^{\mathrm{o}}$, and the minimum communication data, denoted as $l_{\min}^{\mathrm{c}}$, while maintaining the QoS constraints related to the minimum computational and communication requirements for each user through jointly optimizing:

- time allocation variable: $\boldsymbol{\zeta} \triangleq \{\zeta_k[n], k\in\mathcal{K}, n\in\mathcal{N}\}$;
- resource allocation variables: $\mathbf{L} \triangleq \{l_k^{\mathrm{ua}}[n], l_k^{\mathrm{BS}}[n], f_k^{\mathrm{ua}}[n], f_k^{\mathrm{BS}}[n], k\in\mathcal{K}, n\in\mathcal{N}\}$;

- joint active and passive beamforming variables: $\mathbf{W} \triangleq \{\mathbf{w}_k[n], k \in \mathcal{K}, n \in \mathcal{N}\}$ and $\mathbf{\Gamma} \triangleq \{\mathbf{U}_{\rm r}[n], \mathbf{U}_{\rm t}[n], k \in \mathcal{K}, n \in \mathcal{N}\}$, respectively;
- UAV trajectory variable: $\mathbf{Q} \triangleq \{\mathbf{q}_{\rm ua}[n], k \in \mathcal{K}, n \in \mathcal{N}\}$.

Then the optimization problem can be formulated as

$$\max_{\boldsymbol{\zeta},\mathbf{L},\mathbf{W},\mathbf{\Gamma},\mathbf{Q}} \omega_{\rm o} l^{\rm o}_{\min} + \omega_{\rm c} l^{\rm c}_{\min},$$

$$\text{s.t.} \quad (1)-(5),(14)-(16), \tag{17a}$$

$$\delta_{\rm t}\zeta_k[n] R^{\rm ua}_k[n] \geq l^{\rm ua}_k[n], \forall k \in \mathcal{K}, n \in \mathcal{N}, \tag{17b}$$

$$\delta_{\rm t}\zeta_k[n] R^{\rm BS}_k[n] \geq l^{\rm BS}_k[n], \forall k \in \mathcal{K}, n \in \mathcal{N}, \tag{17c}$$

$$l^{\rm o}_{\min} \geq L_{\rm o}, l^{\rm c}_{\min} \geq L_{\rm c}, \tag{17d}$$

$$f^{\rm ua}_k[1] = f^{\rm BS}_k[1] = l^{\rm ua}_k[N] = l^{\rm BS}_k[N] = 0, \forall k \in \mathcal{K}, \tag{17e}$$

$$\beta^m_{\rm r}[n] + \beta^m_{\rm t}[n] = 1, \forall m \in \mathcal{M}, n \in \mathcal{N}, \tag{17f}$$

$$\beta^m_{\rm r}[n], \beta^m_{\rm t}[n] \in (0,1), \forall m \in \mathcal{M}, n \in \mathcal{N}, \tag{17g}$$

$$\phi^m_{\rm r}[n], \phi^m_{\rm t}[n] \in [0, 2\pi), \forall m \in \mathcal{M}, n \in \mathcal{N}, \tag{17h}$$

where $\omega_{\rm o}+\omega_{\rm c} = 1$, $\omega_{\rm o} \in (0,1)$ and $\omega_{\rm c} \in (0,1)$ are the weighted factors that influence the precedence of the computing-focused and communication-focused services, respectively. In fact, the optimization problem (17) poses a significant challenge as it is a non-convex max-min problem, making it difficult to solve directly using conventional convex optimization algorithms. To address this issue, we first introduce two auxiliary variables, $\widehat{l}_{\rm o}$ and $\widehat{l}_{\rm c}$, in place of $l^{\rm o}_{\min}$ and $l^{\rm c}_{\min}$, respectively. This substitution allows for the transformation of the max-min optimization problem into an equivalent max optimization problem. The transformed optimization problem can be re-expressed as

$$\max_{\boldsymbol{\zeta},\mathbf{L},\mathbf{W},\mathbf{\Gamma},\mathbf{Q},\widehat{l}_{\rm o},\widehat{l}_{\rm c}} \omega_{\rm o}\widehat{l}_{\rm o} + \omega_{\rm c}\widehat{l}_{\rm c},$$

$$\text{s.t.} \quad (1)-(5),(14)-(16),(17e)-(17h), \tag{18a}$$

$$\delta_{\rm t}\zeta_k[n] R^{\rm ua}_k[n] \geq l^{\rm ua}_k[n], \forall k \in \mathcal{K}, n \in \mathcal{N}, \tag{18b}$$

$$\delta_{\rm t}\zeta_k[n] R^{\rm BS}_k[n] \geq l^{\rm BS}_k[n], \forall k \in \mathcal{K}, n \in \mathcal{N}, \tag{18c}$$

$$\widehat{l}_{\rm o} \geq L_{\rm o}, \widehat{l}_{\rm o} \leq \sum_{n=1}^{N} l^{\rm ua}_k[n] + l^{\rm BS}_k[n], \ \forall k \in \mathcal{K}, \tag{18d}$$

$$\widehat{l}_{\rm c} \geq L_{\rm c}, \widehat{l}_{\rm c} \leq \sum_{n=1}^{N} \delta_{\rm t}(1-\zeta_k[n]) R^{\rm BS}_k[n], \ \forall k \in \mathcal{K}. \tag{18e}$$

The transformation of the optimization problem (18) into a maximization problem has been accomplished; however, the challenge persists as a non-convex problem due to the absence of convexity in the constraints (18b), (18c), and (18e). Additionally, the distinctive amplitude equality constraints in (17f), induced by the modulation attribute of STAR-RIS for the incoming signals, further contribute to the non-convexity issue. To address this challenge, an alternative approach is employed to decompose the optimization problem (18) into four subproblems by alternatively optimizing the variable subsets $\mathbf{W}$, $\mathbf{\Xi}_1 = \{\mathbf{L}, \boldsymbol{\zeta}, \widehat{l}_{\rm o}, \widehat{l}_{\rm c}\}$, $\mathbf{\Xi}_2 = \{\mathbf{L}, \mathbf{\Gamma}, \widehat{l}_{\rm o}, \widehat{l}_{\rm c}\}$, $\mathbf{\Xi}_3 = \{\mathbf{L}, \mathbf{Q}, \widehat{l}_{\rm o}, \widehat{l}_{\rm c}\}$.

B. Algorithm Design

1) Design $\mathbf{W}$ with the given $\mathbf{\Xi}_1$, $\mathbf{\Xi}_3$ and $\mathbf{\Xi}_3$: Our initial focus is on optimizing the active beamforming variable $\mathbf{W}$ while considering the specified resource allocation $\mathbf{L}$, time scheduling $\boldsymbol{\zeta}$, passive beamforming $\mathbf{\Gamma}$, and UAV trajectory $\mathbf{Q}$. This allows us to streamline the original optimization problem (18) as the following form

$$\max_{\mathbf{W}} \ \sum_{n=1}^{N}\sum_{k=1}^{K} R^{\rm BS}_k[n],$$

$$\text{s.t.} \ \ \|\mathbf{w}_k[n]\| = 1, \ \forall k \in \mathcal{K}, n \in \mathcal{N}. \tag{19a}$$

Actually, the equation (19) can be segmented into $N \times K$ independent sub-problems. Consequently, the approach to resolving the optimization problem (19) can be seen as addressing the $N \times K$ sub-problems concurrently. In terms of $\forall k \in \mathcal{K}, n \in \mathcal{N}$, the subproblem can be expressed as

$$\max_{\mathbf{w}_k[n]} \ \frac{\mathbf{w}^H_k[n]\mathbf{V}_k[n]\mathbf{w}_k[n]}{\mathbf{w}^H_k[n]\mathbf{V}_{-k}[n]\mathbf{w}_k[n]},$$

$$\text{s.t.} \ \ \|\mathbf{w}_k[n]\| = 1, \tag{20a}$$

where we define

- $\mathbf{V}_k[n] = p_{\rm u}\mathbf{H}^H_{\rm BR}[n]\mathbf{U}^H_{\rm r}[n]\mathbf{h}_{{\rm u}k}[n](\mathbf{H}^H_{\rm BR}[n]\mathbf{U}^H_{\rm r}[n]\mathbf{h}_{{\rm u}k}[n])^H$;
- $\mathbf{V}_{-k}[n] = \sigma^2_{\rm BS}\mathbf{I}_{N_{\rm t}} + p_{\rm u}\sum_{j\neq k}^{K}\mathbf{H}^H_{\rm BR}[n]\mathbf{U}^H_{\rm r}[n]\mathbf{h}_{{\rm u}j}[n]\times (\mathbf{H}^H_{\rm BR}[n]\mathbf{U}^H_{\rm r}[n]\mathbf{h}_{{\rm u}j}[n])^H$.

Note that, the closed-form solution for the subproblem (20) can be derived utilizing Theorem 1.

Theorem 1. *It is easy to demonstrate that subproblem* (20) *is a generalized Rayleigh quotient problem [34]. Thus, the optimal solution of the problem* (20) *can be derived as*

$$\mathbf{w}^{\rm opt}_k[n] = \frac{\mathbf{C}^{-H}[n]\tilde{\mathbf{w}}^{\rm opt}_k[n]}{\left\|\mathbf{C}^{-H}[n]\tilde{\mathbf{w}}^{\rm opt}_k[n]\right\|}, \tag{21}$$

where matrix $\mathbf{C}[n]$ is the Cholesky deposition of $\mathbf{V}_{-k}[n]$, $\tilde{\mathbf{w}}^{\rm opt}_k[n] = \text{eigvector}\left\{\max\left\{\text{eig}\left\{\mathbf{C}^{-1}[n]\mathbf{V}_k[n]\mathbf{C}^{-H}[n]\right\}\right\}\right\}$.

Proof: The proof of Theorem 1 is in Appendix A. ■

2) Design $\mathbf{\Xi}_1$ with the given $\mathbf{W}$, $\mathbf{\Upsilon}$ and $\mathbf{Q}$: After obtaining $\mathbf{W}$, we focus on designing the time scheduling variable $\boldsymbol{\zeta}$ and resource allocation variable $\mathbf{L}$ with the given $\mathbf{\Gamma}$ and $\mathbf{Q}$. In particular, the optimization problem associated with $\mathbf{\Xi}_1$ can be formulated as follows:

$$\max_{\mathbf{\Xi}_1} \ \omega_{\rm o}\widehat{l}_{\rm o} + \omega_{\rm c}\widehat{l}_{\rm c},$$

$$\text{s.t.} \quad (1),(2),(14)-(16),(17e), \tag{22a}$$

$$\delta_{\rm t}\zeta_k[n] R^{\rm ua}_k[n] \geq l^{\rm ua}_k[n], \ \forall k \in \mathcal{K}, n \in \mathcal{N}, \tag{22b}$$

$$\delta_{\rm t}\zeta_k[n] R^{\rm BS}_k[n] \geq l^{\rm BS}_k[n], \ \forall k \in \mathcal{K}, n \in \mathcal{N}, \tag{22c}$$

$$\widehat{l}_{\rm o} \geq L_{\rm o}, \widehat{l}_{\rm o} \leq \sum_{n=1}^{N} l^{\rm ua}_k[n] + l^{\rm BS}_k[n], \ \forall k \in \mathcal{K}, \tag{22d}$$

$$\widehat{l}_{\rm c} \geq L_{\rm c}, \widehat{l}_{\rm c} \leq \sum_{n=1}^{N} \delta_t(1-\zeta_k[n]) R^{\rm BS}_k[n], \ \forall k \in \mathcal{K}. \tag{22e}$$

It is worth noting that the optimization problem (22) is a conventional linear programming problem, indicating that the

existing convex optimization tools such as the CVX solver can be effectively utilized to address this issue.

3) Design $\mathbf{\Xi}_2$ with the given $\mathbf{W}$, $\boldsymbol{\zeta}$ and $\mathbf{Q}$: Next, we prioritize the design of $\mathbf{\Gamma}$ based on the provided parameters, i.e., $\mathbf{W}$, $\boldsymbol{\zeta}$ and $\mathbf{Q}$. In particular, the optimization issue related to $\mathbf{\Xi}_2$ can be formulated as:

$$\begin{aligned}
\max_{\mathbf{\Xi}_2} \quad & \omega_{\rm o}\widehat{l_{\rm o}} + \omega_{\rm c}\widehat{l_{\rm c}}, \\
\text{s.t.} \quad & (14)-(16), (17e)-(17h), && \text{(23a)}\\
& \delta_{\rm t}\zeta_k[n]R_k^{\rm ua}[n] \geq l_k^{\rm ua}[n],\ \forall k \in \mathcal{K}, n \in \mathcal{N}, && \text{(23b)}\\
& \delta_{\rm t}\zeta_k[n]R_k^{\rm BS}[n] \geq l_k^{\rm BS}[n],\ \forall k \in \mathcal{K}, n \in \mathcal{N}, && \text{(23c)}\\
& \widehat{l_{\rm o}} \geq L_{\rm o}, \widehat{l_{\rm o}} \leq \sum_{n=1}^{N} l_k^{\rm ua}[n] + l_k^{\rm BS}[n],\ \forall k \in \mathcal{K}, && \text{(23d)}\\
& \widehat{l_{\rm c}} \geq L_{\rm c}, \widehat{l_{\rm c}} \leq \sum_{n=1}^{N} \delta_t(1-\zeta_k[n])R_k^{\rm BS}[n],\ \forall k \in \mathcal{K}. && \text{(23e)}
\end{aligned}$$

Actually, the main challenge of solving the optimization problem (23) lies in the equality constraints involving amplitude coefficients in constraint (17f). These amplitude coefficients are coupled with phase shifts, making it difficult to solve the amplitude coefficients individually. This undeniably increases the complexity of the problem, rendering the common algorithms such as maximum mean-square error (MMSE) challenging to apply directly. To handle this challenge, we leverage the SDR method [35]. Specifically, let $\mathbf{Y}_{\rm r}[n] = \mathbf{u}_{\rm r}\mathbf{u}_{\rm r}^H$ and $\mathbf{Y}_{\rm t}[n] = \mathbf{u}_{\rm t}\mathbf{u}_{\rm t}^H$, where $\mathbf{u}_{\rm r} = \mathrm{diag}(\mathbf{U}_{\rm r})$ and $\mathbf{u}_{\rm t} = \mathrm{diag}(\mathbf{U}_{\rm t})$. Hence, the optimization problem (23) can be transformed as

$$\begin{aligned}
\max_{\mathbf{L},\mathbf{Y}_{\rm r}[n],\mathbf{Y}_{\rm t}[n]} \quad & \omega_{\rm o}\widehat{l_{\rm o}} + \omega_{\rm c}\widehat{l_{\rm c}}, \\
\text{s.t.} \quad & (14)-(16), (17e), && \text{(24a)}\\
& \delta_{\rm t}\zeta_k[n]R_k^{\rm ua}[n] \geq l_k^{\rm ua}[n],\ \forall k \in \mathcal{K}, n \in \mathcal{N}, && \text{(24b)}\\
& \delta_{\rm t}\zeta_k[n]R_k^{\rm BS}[n] \geq l_k^{\rm BS}[n],\ \forall k \in \mathcal{K}, n \in \mathcal{N}, && \text{(24c)}\\
& \widehat{l_{\rm o}} \geq L_{\rm o}, \widehat{l_{\rm o}} \leq \sum_{n=1}^{N} l_k^{\rm ua}[n] + l_k^{\rm BS}[n],\ \forall k \in \mathcal{K}, && \text{(24d)}\\
& \widehat{l_{\rm c}} \geq L_{\rm c}, \widehat{l_{\rm c}} \leq \sum_{n=1}^{N} \delta_t(1-\zeta_k[n])R_k^{\rm BS}[n],\ \forall k \in \mathcal{K}, && \text{(24e)}\\
& \mathrm{diag}(\mathbf{Y}_{\rm r}[n]) + \mathrm{diag}(\mathbf{Y}_{\rm t}[n]) = \mathbf{I}_M,\ \forall n \in \mathcal{N}, && \text{(24f)}\\
& \mathbf{Y}_{\rm r}[n] \succeq 0, \mathbf{Y}_{\rm t}[n] \succeq 0,\ \forall n \in \mathcal{N}, && \text{(24g)}\\
& \mathrm{rank}(\mathbf{Y}_{\rm r}[n]) = \mathrm{rank}(\mathbf{Y}_{\rm t}[n]) = 1,\ \forall n \in \mathcal{N}, && \text{(24h)}
\end{aligned}$$

where, $R_k^{\rm BS}[n]$ and $R_k^{\rm ua}[n]$ can be re-expressed as

$$R_k^{\rm BS}[n] = B\log_2\Big(\frac{\mathrm{Tr}\left(\mathbf{Y}_{\rm r}[n](\mathbf{G}_k^T[n]\circ\mathbf{D}[n])\right)+\sigma_{\rm BS}^2\left\|\mathbf{w}_k\right\|^2}{\mathrm{Tr}\left(\mathbf{Y}_{\rm r}[n](\mathbf{G}_k^T[n]\circ\tilde{\mathbf{D}}_k[n])\right)+\sigma_{\rm BS}^2\left\|\mathbf{w}_k\right\|^2}\Big), \quad (25)$$

$$R_k^{\rm ua}[n] = B\log_2\Big(\frac{\mathrm{Tr}\left(\mathbf{Y}_{\rm t}[n]\big(\mathbf{F}^T\circ\mathbf{D}[n]\big)\right)+\sigma_{\rm ua}^2}{\mathrm{Tr}\left(\mathbf{Y}_{\rm t}[n]\big(\mathbf{F}^T\circ\tilde{\mathbf{D}}_k[n]\big)\right)+\sigma_{\rm ua}^2}\Big), \quad (26)$$

with

- $\mathbf{G}_k[n] = \mathbf{H}_{\rm BR}[n]\mathbf{w}_k[n]\mathbf{w}_k^H[n]\mathbf{H}_{\rm BR}^H[n]$,
- $\mathbf{D}[n] = p_{\rm u}\mathbf{H}_{\rm us}[n]\mathbf{H}_{\rm us}^H[n]$,
- $\tilde{\mathbf{D}}_k[n] = p_{\rm u}\mathbf{H}_{\rm us}[n]\mathbf{A}_{-k}\mathbf{H}_{\rm us}^H[n]$,
- $\mathbf{H}_{\rm us}[n] = \big[\mathbf{h}_{\mathbf{u}1}[n], \cdots, \mathbf{h}_{\mathbf{u}k}[n], \cdots, \mathbf{h}_{\mathbf{u}K}[n]\big]$,
- $\mathbf{A}_{-k} = \mathbf{E}_{-k}\mathbf{E}_{-k}^T$, $\mathbf{F} = \mathbf{h}_{\rm ru}\mathbf{h}_{\rm ru}^H$.

It is worth noting that with the assistance of the SDR method, we can transform the complex equality constraints into convex, i.e., (24f), with respect to (w.r.t.) the variables $\mathbf{Y}_{\rm r}[n]$ and $\mathbf{Y}_{\rm t}[n]$, allowing a holistic solution to be obtained for the reflection and transmission coefficients. Furthermore, the SDR method simplifies the complex achievable rate functions into relatively simpler forms w.r.t. $\mathbf{Y}_{\rm r}[n]$ and $\mathbf{Y}_{\rm t}[n]$.

In fact, the problem (24) is still a non-convex optimization problem, due to the fact that $R_k^{\rm BS}[n]$ and $R_k^{\rm ua}[n]$ are respectively non-convex function w.r.t. $\mathbf{Y}_{\rm r}[n]$ and $\mathbf{Y}_{\rm t}[n]$, and the non-convex rank-one constraints in (24h). To address this problem, we first employ the simple successive convex approximation (SCA) technique, i.e., first-order Taylor expansion, to derive the concave lower bound of $R_k^{\rm BS}[n]$ and $R_k^{\rm ua}[n]$ in the $(i+1)$-th inner loop iteration of the proposed iterative algorithm. And their lower bounds will be leveraged to replace themselves to obtain an approximately convex optimization problem. The lower bounds can be derived as

$$\begin{aligned}
R_k^{\rm BS}[n] \geq \tilde{R}_k^{\rm BS}[n] = &-\hat{f}_1\big(\mathbf{Y}_{\rm r}^{(i)}[n], \mathbf{Y}_{\rm r}[n]\big) + \\
&\log_2\left(\mathrm{Tr}\left(\mathbf{Y}_{\rm r}[n](\mathbf{G}_k^T[n]\circ\mathbf{D}[n])\right)+\sigma_{\rm BS}^2\left\|\mathbf{w}_k\right\|^2\right), \quad (27)
\end{aligned}$$

$$\begin{aligned}
R_k^{\rm ua}[n] \geq \tilde{R}_k^{\rm ua}[n] = &-\hat{f}_2\big(\mathbf{Y}_{\rm t}^{(i)}[n], \mathbf{Y}_{\rm t}[n]\big) + \\
&\log_2\left(\mathrm{Tr}\left(\mathbf{Y}_{\rm t}[n](\mathbf{F}^T\circ\mathbf{D}[n])\right)+\sigma_{\rm ua}^2\right), \quad (28)
\end{aligned}$$

where the expression of $\hat{f}_1$ and $\hat{f}_2$ are respectively given in (29) and (30), which are shown at the top of the next page.

Then, we employ an equivalent form of the rank-one constraints [24] to replace them, which can be expressed as

$$\mathrm{rank}(\mathbf{Y}_\epsilon[n]) = 1 \Leftrightarrow \mathrm{Tr}(\mathbf{Y}_\epsilon[n]) - \left\|\mathbf{Y}_\epsilon[n]\right\|_2 = 0. \quad (31)$$

It is important to note that the equivalent form of the rank-one constraint is a non-convex constraint. Additionally, for any positive semidefinite matrix $\mathbf{Z}$, $\mu(\mathbf{Z}) = \mathrm{Tr}(\mathbf{Z}) - \left\|\mathbf{Z}\right\|_2 \geq 0$ always holds and the equality is satisfied if and only if $\mathrm{rank}(\mathbf{Z}) = 1$. Thus, we transform the equality constraint into the penalty term subtracted by the objective function based on the non-negative characteristic of μ and devise an inner loop iteration to iteratively enforce the penalty term towards zero. Note that the function $\mu(\mathbf{Z})$ is a concave function w.r.t. $\mathbf{Z}$ due to the convex spectral norm $\left\|\mathbf{Z}\right\|_2$, which makes the optimization problem with penalty term is a non-convex problem. In order to handle this problem, the linear lower bound of the spectral norm is utilized to replace itself. The expression for the upper bound of the penalty term $\mu(\mathbf{Y}_\varsigma[n])$ in the $(i+1)$-th iteration of the inner loop can be given as:

$$\begin{aligned}
\mu(\mathbf{Y}_\epsilon[n]) \leq \widehat{\mu}_\epsilon(\mathbf{Y}_\epsilon[n], \mathbf{Y}_\epsilon^{(i)}[n]) = \mathrm{Tr}(\mathbf{Y}_\epsilon[n]) - \Big(\Big\|\mathbf{Y}_\epsilon^{(i)}[n]\Big\|_2 \\
+ \mathrm{Tr}(\mathbf{y}_\epsilon^{(i)}[n](\mathbf{y}_\epsilon^{(i)}[n])^H)(\mathbf{Y}_\epsilon - \mathbf{Y}_\epsilon^{(i)}[n])\Big),\ \forall n \in \mathcal{N}, \quad (32)
\end{aligned}$$

where $\mathbf{y}_\epsilon^{(i)}[n]$ denotes the eigenvector associated with the largest eigenvalue of $\mathbf{Y}_\epsilon^{(i)}[n]$.

$$\hat{f}_1\big(\mathbf{Y}_{\mathrm{r}}^{(i)}[n],\mathbf{Y}_{\mathrm{r}}[n]\big)=B\Big(\frac{\mathrm{Tr}\left(\mathbf{Y}_{\mathrm{r}}[n](\mathbf{G}_k^T[n]\circ\tilde{\mathbf{D}}_k[n])\right)-\mathrm{Tr}\left(\mathbf{Y}_{\mathrm{r}}^{(i)}[n](\mathbf{G}_k^T[n]\circ\tilde{\mathbf{D}}_k[n])\right)}{\ln^2\left(\mathrm{Tr}\left(\mathbf{Y}_{\mathrm{r}}^{(i)}[n](\mathbf{G}_k^T[n]\circ\tilde{\mathbf{D}}_k[n])\right)+\sigma_{\mathrm{BS}}^2\left\|\mathbf{w}_k\right\|^2\right)}+\log_2\left(\mathrm{Tr}\left(\mathbf{Y}_{\mathrm{r}}^{(i)}[n](\mathbf{G}_k^T[n]\circ\tilde{\mathbf{D}}_k[n])\right)+\sigma_{\mathrm{BS}}^2\left\|\mathbf{w}_k\right\|^2\right)\Big), \tag{29}$$

$$\hat{f}_2\big(\mathbf{Y}_{\mathrm{r}}^{(i)}[n],\mathbf{Y}_{\mathrm{r}}[n]\big)=B\Big(\frac{\mathrm{Tr}\left(\mathbf{Y}_{\mathrm{t}}[n]\big(\mathbf{F}^T\circ\tilde{\mathbf{D}}_k[n]\big)\right)-\mathrm{Tr}\left(\mathbf{Y}_{\mathrm{t}}^{(i)}[n]\big(\mathbf{F}^T\circ\tilde{\mathbf{D}}_k[n]\big)\right)}{\ln^2\left(\mathrm{Tr}\left(\mathbf{Y}_{\mathrm{t}}^{(i)}[n]\big(\mathbf{F}^T\circ\tilde{\mathbf{D}}_k[n]\big)\right)+\sigma_{\mathrm{ua}}^2\right)}+\log_2\left(\mathrm{Tr}\left(\mathbf{Y}_{\mathrm{t}}^{(i)}[n]\big(\mathbf{F}^T\circ\tilde{\mathbf{D}}_k[n]\big)\right)+\sigma_{\mathrm{ua}}^2\right)\Big). \tag{30}$$

Consequently, the optimization problem (24) in the $(i+1)$-th innerloop iteration can be expressed as the following problem:

$$\begin{aligned}
\max_{\mathbf{L},\mathbf{Y}_{\mathrm{r}}[n],\mathbf{Y}_{\mathrm{t}}[n]}\ & \omega_{\mathrm{o}}\widehat{l}_{\mathrm{o}}+\omega_{\mathrm{c}}\widehat{l}_{\mathrm{c}}-\sum_{n=1}^{N}(\varrho_{\mathrm{r}}\widehat{\mu}_{\mathrm{r}}(\mathbf{Y}_{\mathrm{r}}[n],\mathbf{Y}_{\mathrm{r}}^{(i)}[n])\\
&+\varrho_{\mathrm{t}}\widehat{\mu}_{\mathrm{t}}(\mathbf{Y}_{\mathrm{t}}[n],\mathbf{Y}_{\mathrm{t}}^{(i)}[n])),\\
\text{s.t.}\ & (14)-(16),(17\mathrm{e}), && \text{(33a)}\\
& \delta_{\mathrm{t}}\zeta_k[n]\tilde{R}_k^{\mathrm{ua}}[n]\geq l_k^{\mathrm{ua}}[n],\ \forall k\in\mathcal{K},n\in\mathcal{N}, && \text{(33b)}\\
& \delta_{\mathrm{t}}\zeta_k[n]\tilde{R}_k^{\mathrm{BS}}[n]\geq l_k^{\mathrm{BS}}[n],\ \forall k\in\mathcal{K},n\in\mathcal{N}, && \text{(33c)}\\
& \widehat{l}_{\mathrm{o}}\geq L_{\mathrm{o}},\widehat{l}_{\mathrm{o}}\leq\sum_{n=1}^{N}l_k^{\mathrm{ua}}[n]+l_k^{\mathrm{BS}}[n],\ \forall k\in\mathcal{K}, && \text{(33d)}\\
& \widehat{l}_{\mathrm{c}}\geq L_{\mathrm{c}},\widehat{l}_{\mathrm{c}}\leq\sum_{n=1}^{N}\delta_t(1-\zeta_k[n])\tilde{R}_k^{\mathrm{BS}}[n],\ \forall k\in\mathcal{K}, && \text{(33e)}\\
& \mathrm{diag}(\mathbf{Y}_{\mathrm{r}}[n])+\mathrm{diag}(\mathbf{Y}_{\mathrm{t}}[n])=\mathbf{I}_M,\ \forall n\in\mathcal{N}, && \text{(33f)}\\
& \mathbf{Y}_{\mathrm{r}}[n]\succeq 0,\ \mathbf{Y}_{\mathrm{t}}[n]\succeq 0,\ \forall n\in\mathcal{N}, && \text{(33g)}
\end{aligned}$$

where ϱ_{r} and ϱ_{t} are the penalty coefficients for the rank-one constraints. During the optimization process, we progressively increase the values of $\varrho_{\mathrm{r}}>0$ and $\varrho_{\mathrm{t}}>0$ to compel $\widehat{\mu}(\mathbf{Y}_{\mathrm{r}}[n],\mathbf{Y}_{\mathrm{r}}^{(i)}[n])$ and $\widehat{\mu}(\mathbf{Y}_{\mathrm{t}}[n],\mathbf{Y}_{\mathrm{t}}^{(i)}[n])$ towards zero, thereby achieving the rank-one resolution.

Note that the problem (33) is a conventional convex semidefinite programming (SDP) that can be efficiently resolved with the use of CVX.

4) Design $\mathbf{\Xi}_3$ with the given $\mathbf{W}$, $\boldsymbol{\zeta}$ and $\mathbf{\Gamma}$: We then shift our attention to designing $\mathbf{Q}$ using the optimized $\mathbf{W}$, $\boldsymbol{\zeta}$, and $\mathbf{\Gamma}$. More specifically, the optimization problem associated with $\mathbf{\Xi}_3$ can be formulated as:

$$\begin{aligned}
\max_{\mathbf{\Xi}_3}\ & \omega_{\mathrm{o}}\widehat{l}_{\mathrm{o}}+\omega_{\mathrm{c}}\widehat{l}_{\mathrm{c}},\\
\text{s.t.}\ & (3)-(5),(14)-(16),(17\mathrm{e}), && \text{(34a)}\\
& \delta_{\mathrm{t}}\zeta_k[n]R_k^{\mathrm{ua}}[n]\geq l_k^{\mathrm{ua}}[n],\forall k\in\mathcal{K},n\in\mathcal{N}, && \text{(34b)}\\
& \delta_{\mathrm{t}}\zeta_k[n]R_k^{\mathrm{BS}}[n]\geq l_k^{\mathrm{BS}}[n],\forall k\in\mathcal{K},n\in\mathcal{N}, && \text{(34c)}\\
& \widehat{l}_{\mathrm{o}}\geq L_{\mathrm{o}},\widehat{l}_{\mathrm{o}}\leq\sum_{n=1}^{N}l_k^{\mathrm{ua}}[n]+l_k^{\mathrm{BS}}[n],\ \forall k\in\mathcal{K}, && \text{(34d)}\\
& \widehat{l}_{\mathrm{c}}\geq L_{\mathrm{c}},\widehat{l}_{\mathrm{c}}\leq\sum_{n=1}^{N}\delta_t(1-\zeta_k[n])R_k^{\mathrm{BS}}[n],\ \forall k\in\mathcal{K}. && \text{(34e)}
\end{aligned}$$

Actually, due to the fact that $R_k^{\mathrm{BS}}[n]$ and $R_k^{\mathrm{ua}}[n]$ are the non-convex function w.r.t. UAV's trajectory variable $\mathbf{Q}$ and $\mathbf{Q}$ is strongly coupled with channel, it is challenging to tackle this optimization problem. To address this challenge, we initially introduce the appropriate auxiliary variables $\lambda_k[n]$ and $\tilde{\lambda}[n]$ with $\lambda_k[n]=\frac{1}{\|\mathbf{q}_{\mathrm{ua}}[n]-\mathbf{q}_k\|^{\alpha_{\mathrm{uk}}}}$ and $\tilde{\lambda}[n]=\|\mathbf{q}_{\mathrm{ua}}[n]-\mathbf{q}_{\mathrm{BS}}\|^{\alpha_{\mathrm{BR}}}$ to restructure the expressions of the communication rates. In particular, $R_k^{\mathrm{ua}}[n]$ and $R_k^{\mathrm{BS}}[n]$ can be re-written as

$$R_k^{\mathrm{ua}}[n]=\log_2\left(\frac{\mathbf{a}^T[n]\boldsymbol{\lambda}[n]+\sigma_{\mathrm{ua}}^2}{\mathbf{a}^T[n]\mathbf{A}_{-k}\boldsymbol{\lambda}[n]+\sigma_{\mathrm{ua}}^2}\right), \tag{35}$$

$$R_k^{\mathrm{BS}}[n]=\log_2\left(\frac{\mathbf{b}_k^T\boldsymbol{\lambda}[n]+\left\|\mathbf{w}_k\right\|^2\sigma_{\mathrm{BS}}^2\tilde{\lambda}[n]}{\mathbf{b}_k^T\mathbf{A}_{-k}\boldsymbol{\lambda}[n]+\left\|\mathbf{w}_k\right\|^2\sigma_{\mathrm{BS}}^2\tilde{\lambda}[n]}\right), \tag{36}$$

where

- $\mathbf{a}[n]=p_{\mathrm{u}}\rho\Big[\left|\mathbf{h}_{\mathrm{ru}}^H\mathbf{U}_{\mathrm{t}}[n]\widehat{\mathbf{h}}_{\mathrm{u}1}[n]\right|^2,\cdots,\left|\mathbf{h}_{\mathrm{ru}}^H\mathbf{U}_{\mathrm{t}}[n]\widehat{\mathbf{h}}_{\mathrm{u}k}[n]\right|^2,\cdots,\left|\mathbf{h}_{\mathrm{ru}}^H\mathbf{U}_{\mathrm{t}}[n]\widehat{\mathbf{h}}_{\mathrm{u}K}[n]\right|^2\Big]^T$;
- $\mathbf{b}_k[n]=p_{\mathrm{u}}\rho^2\Big[\left|\mathbf{w}_k^H[n]\widehat{\mathbf{H}}_{\mathrm{BR}}^H[n]\mathbf{U}_{\mathrm{r}}^H[n]\widehat{\mathbf{h}}_{\mathrm{u}1}[n]\right|^2,\cdots,\left|\mathbf{w}_k^H[n]\widehat{\mathbf{H}}_{\mathrm{BR}}^H[n]\mathbf{U}_{\mathrm{r}}^H[n]\widehat{\mathbf{h}}_{\mathrm{u}k}[n]\right|^2,\cdots,\left|\mathbf{w}_k^H[n]\widehat{\mathbf{H}}_{\mathrm{BR}}^H[n]\mathbf{U}_{\mathrm{r}}^H[n]\widehat{\mathbf{h}}_{\mathrm{u}K}[n]\right|^2\Big]^T$;
- $\boldsymbol{\lambda}[n]=\{\lambda_1[n],\cdots,\lambda_k[n],\cdots,\lambda_K[n]\}$.

Note that with the help of these auxiliary variables, we can effectively decouple the UAV position variables that originally intertwined in the channel and separate the UAV position variables from the communication rate expressions, effectively streamlining the optimization process.

Then, introducing the variables $g_1[n]$, $g_{2,k}[n]$, $\tilde{g}_{1,k}[n]$ and $\tilde{g}_{2,k}[n]$, which satisfy the following constraints:

$$g_1[n]\leq\mathbf{a}^T[n]\boldsymbol{\lambda}[n]+\sigma_{\mathrm{ua}}^2,\ \forall n\in\mathcal{N}, \tag{37}$$

$$g_{2,k}[n]\geq\mathbf{a}^T[n]\mathbf{A}_{-k}\boldsymbol{\lambda}[n]+\sigma_{\mathrm{ua}}^2,\ \forall k\in\mathcal{K},n\in\mathcal{N}, \tag{38}$$

$$\tilde{g}_{1,k}[n]\leq\mathbf{b}_k^T\boldsymbol{\lambda}[n]+\left\|\mathbf{w}_k\right\|^2\sigma_{\mathrm{BS}}^2\tilde{\lambda}[n],\ \forall k\in\mathcal{K},n\in\mathcal{N}, \tag{39}$$

$$\tilde{g}_{2,k}[n]\geq\mathbf{b}_k^T\mathbf{A}_{-k}\boldsymbol{\lambda}[n]+\left\|\mathbf{w}_k\right\|^2\sigma_{\mathrm{BS}}^2\tilde{\lambda}[n],\ \forall k\in\mathcal{K},n\in\mathcal{N}. \tag{40}$$

Consequently, we can obtain the lower bounds of $R_k^{\mathrm{ua}}[n]$ and $R_k^{\mathrm{BS}}[n]$ in the $(l+1)$-th outer loop iteration, which are respectively given by

- $R_k^{\mathrm{ua}}[n]\geq\log_2\left(\frac{g_1[n]}{g_{2,k}[n]}\right)\geq\log_2\left(g_1[n]\right)-\left(\log_2\left(g_{2,k}^{(l)}[n]\right)+\frac{g_{2,k}[n]-g_{2,k}^{(l)}[n]}{g_{2,k}^{(l)}[n]\ln 2}\right)=\widehat{R}_k^{\mathrm{ua}}$,
- $R_k^{\mathrm{BS}}[n]\geq\log_2\left(\frac{\tilde{g}_{1,k}[n]}{\tilde{g}_{2,k}[n]}\right)\geq\log_2\left(\tilde{g}_{1,k}[n]\right)-\left(\log_2\left(g_{2,k}^{(l)}[n]\right)+\frac{\tilde{g}_{2,k}[n]-\tilde{g}_{2,k}^{(l)}[n]}{\tilde{g}_{2,k}^{(l)}[n]\ln 2}\right)=\widehat{R}_k^{\mathrm{BS}}$.

In terms of the non-convex equality constraints $\lambda_k[n] = \frac{1}{\|\mathbf{q}_{\rm ua}[n]-\mathbf{q}_k\|^{\alpha_{{\rm u}k}}}$ and $\tilde{\lambda}[n] = \|\mathbf{q}_{\rm ua}[n]-\mathbf{q}_{\rm BS}\|^{\alpha_{\rm BR}}$, we equivalently reformulate them as

$$\lambda_k[n] \le \frac{1}{\|\mathbf{q}_{\rm ua}[n]-\mathbf{q}_k\|^{\alpha_{{\rm u}k}}}, \tag{41}$$

$$\lambda_k[n] \ge \frac{1}{\|\mathbf{q}_{\rm ua}[n]-\mathbf{q}_k\|^{\alpha_{{\rm u}k}}}, \tag{42}$$

$$\tilde{\lambda}[n] \le \|\mathbf{q}_{\rm ua}[n]-\mathbf{q}_{\rm BS}\|^{\alpha_{\rm BR}}, \tag{43}$$

$$\tilde{\lambda}[n] \ge \|\mathbf{q}_{\rm ua}[n]-\mathbf{q}_{\rm BS}\|^{\alpha_{\rm BR}}. \tag{44}$$

Note that (41), (42) and (43) are still non-convex constraints. To handle these non-convex constraints, the first-order Taylor expansion is adopted to respectively transform them as

$$\|\mathbf{q}_{\rm ua}[n]-\mathbf{q}_k\|^{\alpha_{\rm ua}} \le \frac{1}{\lambda_k^{(l)}[n]} - \frac{\lambda_k[n]-\lambda_k^{(l)}[n]}{(\lambda_k^{(l)}[n])^2}, \tag{45}$$

$$\begin{aligned}\frac{1}{\lambda_k[n]} \le{}& \left\|\mathbf{q}_{\rm ua}^{(l)}[n]-\mathbf{q}_k\right\|^{\alpha_{\rm ua}} + \alpha_{\rm ua}\left(\mathbf{q}_{\rm ua}^{(l)}[n]-\mathbf{q}_k\right)^T \\ &\left(\mathbf{q}_{\rm ua}[n]-\mathbf{q}_{\rm ua}^{(l)}[n]\right)\left\|\mathbf{q}_{\rm ua}^{(l)}[n]-\mathbf{q}_k\right\|^{\alpha_{\rm ua}-2},\end{aligned} \tag{46}$$

$$\begin{aligned}\tilde{\lambda}[n] \le{}& \left\|\mathbf{q}_{\rm ua}^{(l)}[n]-\mathbf{q}_{\rm BS}\right\|^{\alpha_{\rm BS}} + \alpha_{\rm BS}\left(\mathbf{q}_{\rm ua}^{(l)}[n]-\mathbf{q}_{\rm BS}\right)^T \\ &\left(\mathbf{q}_{\rm ua}[n]-\mathbf{q}_{\rm ua}^{(l)}[n]\right)\left\|\mathbf{q}_{\rm ua}^{(l)}[n]-\mathbf{q}_{\rm BS}\right\|^{\alpha_{\rm BS}-2}.\end{aligned} \tag{47}$$

Consequently, the optimization problem described in equation (34) during the $(l+1)$-th iteration of the proposed algorithm can be further transformed as the following convex optimization problem:

$$\max_{\boldsymbol{\Xi}}\ \omega_{\rm o}\widehat{l}_{\rm o} + \omega_{\rm c}\widehat{l}_{\rm c},$$

$$\text{s.t. } (3)-(5),(14)-(16),(17e),(37)-(40),(44)-(47), \tag{48a}$$

$$\delta_{\rm t}\zeta_k[n]\widehat{R}_k^{\rm ua} \ge l_k^{\rm ua}[n], \forall k\in\mathcal{K}, n\in\mathcal{N}, \tag{48b}$$

$$\delta_{\rm t}\zeta_k[n]\widehat{R}_k^{\rm BS} \ge l_k^{\rm BS}[n], \forall k\in\mathcal{K}, n\in\mathcal{N}, \tag{48c}$$

$$\widehat{l}_{\rm o} \ge L_{\rm o}, \widehat{l}_{\rm o} \le \sum_{n=1}^{N} l_k^{\rm ua}[n] + l_k^{\rm BS}[n],\ \forall k\in\mathcal{K}, \tag{48d}$$

$$\widehat{l}_{\rm c} \ge L_{\rm c}, \widehat{l}_{\rm c} \le \sum_{n=1}^{N} \delta_t(1-\zeta_k[n])\widehat{R}_k^{\rm BS}[n],\ \forall k\in\mathcal{K}, \tag{48e}$$

where $\boldsymbol{\Xi} = \{\boldsymbol{\Xi}_3, g_1[n], g_{2,k}[n], \tilde{g}_{1,k}[n], \tilde{g}_{2,k}[n], \lambda_k[n], \tilde{\lambda}[n], k\in\mathcal{K}, n\in\mathcal{N}\}$. This convex optimization problem can be directly solved by leveraging CVX.

C. Designed Algorithm & Analysis on Computational Complexity and Convergence

In this section, the comprehensive examination of the iterative algorithm designed to address the STOC problem with the support of STAR-RIS and UAV is outlined in detail. Specifically, the proposed optimization algorithm is outlined as Algorithm 1, which is a two-tier iterative approach. Within this framework, the inner loop functions to progressively elevate the penalty factors in order to attain rank-one solutions within the third subproblem. Additionally, the parameter $\tilde{v}$ represents the state of fulfilling the rank-one constraints. Specifically, when $\tilde{v}$ dips below a predetermined threshold $\tilde{\varepsilon}$, the inner loop will reach convergence, resulting in the acquisition of the rank-one solutions. Convergence is reached when the discrepancy in the objective function value between consecutive iterations, denoted as v, falls below the predefined threshold ε. The scaling factors $\tilde{\xi}_1 > 0$ and $\tilde{\xi}_2 > 0$ correspond to the penalty coefficients used in the process.

Algorithm 1: Algorithm for STOC Optimization Problem Supported by STAR-RIS and UAV (17)

1: **Initialize**: Feasible point $\left(\mathbf{W}^{(0)}, \mathbf{L}^{(0,0)}, \boldsymbol{\zeta}^{(0)}, \boldsymbol{\Gamma}^{(0,0)}, \mathbf{Q}^{(0)}\right)$; Define the tolerance accuracy thresholds ε and $\tilde{\varepsilon}$; Set the outer iteration index l = 0.
2: **While** $v > \varepsilon$ or $l = 0$ **do**
3: Solve the subproblem (19) with given$\left(\boldsymbol{\zeta}^{(l)}, \boldsymbol{\Gamma}^{(l,0)}, \mathbf{Q}^{(l)}, \mathbf{L}^{(l,0)}\right)$; Update $\mathbf{W}^{(l+1)}$ with the obtained solutions.
4: Solve the subproblem (22) with given$\left(\mathbf{W}^{(l+1)}, \boldsymbol{\Gamma}^{(l,0)}, \mathbf{Q}^{(l)}\right)$; Update $\boldsymbol{\zeta}^{(l+1)}$ and $\mathbf{L}^{(l+1,0)}$ with the obtained solutions.
5: **While** $\tilde{v} > \tilde{\varepsilon}$ or $i = 0$ **do**
6: Solve the optimization problem (23) with the given $\left(\mathbf{W}^{(l+1)}, \boldsymbol{\zeta}^{(l+1)}, \mathbf{Q}^{(l+1)}\right)$; Update $\boldsymbol{\Gamma}^{(l,i+1)}$ and $\mathbf{L}^{(l+1,i+1)}$ with the obtained solutions.
7: Calculate $\tilde{v} = \max\{\widehat{\mu}_{\rm r}, \widehat{\mu}_{\rm t}\}$ based on the acquired solution; Update the penalty coefficients $\varrho_{\rm r}^{(i+1)} = \tilde{\xi}_1\varrho_{\rm r}^{(i)}$, $\varrho_{\rm t}^{(i+1)} = \tilde{\xi}_2\varrho_{\rm t}^{(i)}$; Let $i = i+1$.
8: **end while**
9: Update $(\boldsymbol{\Gamma}^{(l+1,0)}, \mathbf{L}^{(l+1,0)})$ with $(\boldsymbol{\Gamma}^{(l,i)}, \mathbf{L}^{(l+1,i)})$.
10: Solve the optimization problem (34) with the given $\left(\mathbf{W}^{(l+1)}, \boldsymbol{\zeta}^{(l+1)}, \boldsymbol{\Gamma}^{(l+1,0)}, \mathbf{Q}^{(l)}\right)$; Update $\mathbf{Q}^{(l+1)}$ and $\mathbf{L}^{(l+1,0)}$ with the obtained solutions.
11: Calculate the objective value $\overline{R}^{(l+1)} = \omega_{\rm o}\widehat{l}_{\rm o} + \omega_{\rm c}\widehat{l}_{\rm c}$ and update $v = \left|\overline{R}^{(l+1)} - \overline{R}^{(l)}\right|$ based the obtained solutions; Let $l = l+1$.
12: **end while**
13: Output the optimal $\left(\mathbf{W}, \mathbf{L}, \boldsymbol{\zeta}, \boldsymbol{\Gamma}, \mathbf{Q}\right)$.

Next, the analysis of the computing complexity for the proposed algorithm is presented. It is worth noting that the interior point method is utilized to tackle the divided subproblems. In particular, the primary computing complexity of the proposed iterative algorithm arises from addressing subproblems (22), (23) and (34). For the second subproblem, it is a standard linear programming problem. Hence, the computing complexity solving this problem can be expressed as $\mathcal{O}_1 = \mathcal{O}(L(5KN)^{3.5})$, where L denotes the total iteration number of the proposed algorithm. In terms of the the non-convex subproblem (23), it is transformed into a SDP optimization problem, i.e., (33). To obtain the rank-one solutions, a inner loop iteration is employed. Thus, the computing complexity of solving this SDP problem can be expressed as $\mathcal{O}_2 = \mathcal{O}(LL_1(4KN + 2NM^2)^{3.5})$, where L_1 represents the iteration number of the inner loop. The non-convex subproblem (34) is converted into a convex optimization problem (48) by using SCA technology. The computational complexity

associated with solving this problem is primarily characterized by $\mathcal{O}_3 = \mathcal{O}(L(8KN + 2N)^{3.5})$. Consequently, the total computational complexity is given by $\mathcal{O} = \mathcal{O}_1 + \mathcal{O}_2 + \mathcal{O}_3$. According to the obtained analysis results, it is observed that the main computational challenge is associated with the passive beamforming design, and the overall computing complexity of the proposed algorithm is influenced by the number of sub-time slots (N) and the quantity of elements deployed at STAR-RIS (M).

Considering the utilization of the alternative strategy, the proposed iterative algorithm can ensure that every iteration yields a solution at least not worse than the previous one, leading to a monotonically non-decreasing objective function value versus the iterations. Hence, the convergence of the proposed algorithm can always be guaranteed. In addition, the proposed optimization problem is carefully formulated to address the key challenges in UAV-enabled STAR-RIS-aided communication networks, including inter-user interference, diverse QoS requirements, varying service demands, and the priority and fairness of users' service needs. By incorporating these factors, the optimization problem not only ensures a high level of practicality but also demonstrates adaptability to a wide range of real-world scenarios. This formulation provides a valuable reference for the development of optimization models tailored to UAV-assisted communication networks, enabling the accommodation of diverse service requirements and efficient resource management. Consequently, the proposed algorithm for solving this optimization problem is both scalable and adaptable. It is particularly effective in environments where multiple users require simultaneous support for diverse services, such as communication-centric and computation-centric tasks, under varying resource constraints.

IV. Numerical Simulation

To evaluate the effectiveness of the proposed STOC scheme, assisted by STAR-RIS and UAV, alongside the proposed iterative algorithm, we give the numerical simulation results and conduct the comparison analysis with three benchmark schemes, including: **1) RIS-aided scheme:** To obtain the full space coverage,two neighbouring traditional RISs are employed in this scheme, each equipped with half the total elements, one dedicated to reflection and the other to transmission, acting as a replacement for the STAR-RIS system. **2) Without trajectory optimization scheme:** We concentrate on formulating the time scheduling variable $\boldsymbol{\zeta}$, resources allocation variable $\mathbf{L}$, passive beamforming variable $\boldsymbol{\Gamma}$, and UAV trajectory variable $\mathbf{Q}$, while assuming a constant speed for the UAV flying straightly from the initial point to the final point. **3) Equal slot partition scheme:** In this scheme, each time slot in this system is segmented into K uniform partitions, and each partition is designated for one of K users to offload their computational tasks. **4) Uniform energy splitting scheme:** This scheme assumes that all elements equipped at the STAR-RIS employ the same amplitude coefficients for transmission and reflection, respectively, i.e., $\beta_{\mathrm{r}}^m[n] = \beta_{\mathrm{t}}^m[n] = 0.5, \forall m \in \mathcal{M}, n \in \mathcal{N}$. **5) MRT scheme:** In this case, the active beamforming $\{\mathbf{w}_k\}_{k=1}^K$ are designed utilizing the maximum ratio transmission (MRT) algorithm. Additionally, we list the parameters' values associated with the simulations in Table I.

TABLE I
Parameters Setting

Parameters	Symbol and Value
Altitude of UAV	$H = 20$ m
Bandwidth	$B = 1$ MHz
BS position	$\mathbf{q}_{\mathrm{BS}} = [-100, 0, 10]^T$ m
Carrier frequency	$f_{\mathrm{c}} = 2.4$ GHz
Effective capacitance coefficient of MEC servers	$\iota_{\mathrm{ua}} = \iota_{\mathrm{BS}} = 10^{-27}$
Initial/final point of UAV trajectory	$\mathbf{q}_{\mathrm{I}} = [0, 100, 20]^T$ m, $\mathbf{q}_{\mathrm{F}} = [0, -100, 20]^T$ m
Maximum flight velocity and acceleration of UAV	$v_{\max} = 30$ m/s, $a_{\max} = 50$ m/s^2
Maximum CPU frequency	$F_{\mathrm{BS}} = 20$ GHz, $F_{\mathrm{ua}} = 6$ GHz
Noise power	$\sigma_{\mathrm{ua}}^2 = \sigma_{\mathrm{BS}}^2 = -100$ dBm
Pass loss exponent	$\alpha_{\mathrm{u}k} = 2.6$, $\alpha_{\mathrm{BR}} = 2.1$
Rician factor	$\beta = 20$ dB
Scaling factor	$\tilde{\xi}_1 = \tilde{\xi}_2 = 10$
CPU cycles required to process 1 bit of data	$\varrho_{\mathrm{ua}} = \varrho_{\mathrm{BS}} = 10^3$ cycles/bit
Time slot	$\delta_{\mathrm{t}} = 0.3$ s
Transmitting power at users	$p_{\mathrm{u}} = 20$ dBm
Tolerance accuracy thresholds	$\varepsilon = \tilde{\varepsilon} = 10^{-3}$

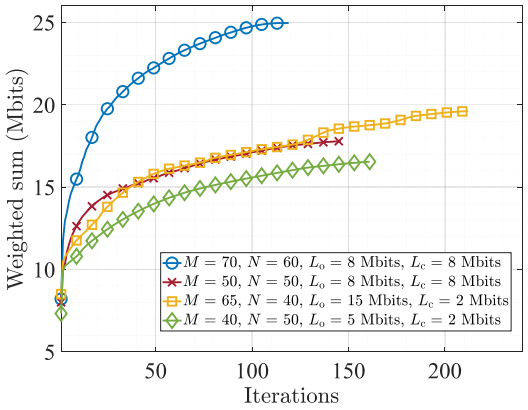

Fig. 3. Weighted sum versus iterations

First, we show the convergence curves of the proposed algorithm taking account of different number of elements (M) and time slots (N), as well as different QoS requirements (L_{o} and L_{c}), as shown in Fig. 3. In particular, it is observed that the weighted sum steadily rises with each iteration, ultimately reaching a stable value. This illustrates the reliable convergence of the proposed iterative algorithm. Generally, the algorithm under consideration consistently demonstrates the ability to swiftly attain a significantly high objective function value as the iteration proceeds, and gradually approaching stable values after several iterations across all scenarios.

Fig. 4 illustrates the trajectory of the UAV while taking into account various QoS requirements related to the minimal

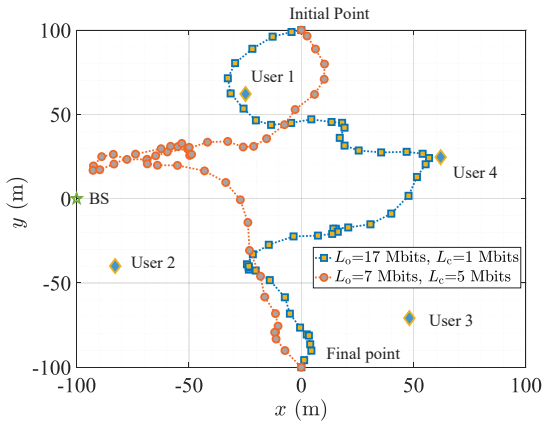

Fig. 4. UAV trajectory with $M = 50$, $N = 50$, $N_t = 6$, $\omega_o = \omega_c = 0.5$, as well as the different L_o and L_c.

quantities of offloaded data and communicational data, i.e., L_o and L_c. In particular, the UAV will strive to approach each user when there is a significant need for task offloading but a small communication requirement for each user, aiming to establish an efficient communication channel to enhance the task offloading rate from users to the MEC server onboard the UAV. Note that, although the UAV's attempt to reach each user may result in an increased distance between the UAV and the BS, hindering the enhancement of users' communication capabilities, it can still effectively meet the minimal communication needs. Given that users transmit their data to the BS via the reflective capabilities of the STAR-RIS deployed on the UAV, the transmitted signal is subject to significant path loss prior to reaching the BS. To meet the growing demands of communications, the UAV try to select an optimized flying path between users and the BS so as to enhance the quality of the effective communication channels, thereby boosting the communication rates while fulfilling the task offloading necessities of multiple users.

The altered correlation of the weighted sum between l^{o}_{min} and l^{c}_{min} with the number of elements deployed at the STAR-RIS can be observed in Fig. 5. Based on the simulation findings, it is evident that the weight sum of the computing and communication data increases progressively as M grows across all scenarios. This phenomenon can be attributed to the fact that a larger number of elements offer greater flexibility to reconfigure the propagation environment. Nevertheless, the rate of this increase falls as the number of elements integrated at the STAR-RIS rises, which is due to the limitation of the system setting. It is important to highlight that the proposed MEC scheme exhibits superior performance gain compared to five other benchmark MEC schemes. The reasons can be concluded as: (i) Compared with the proposed MEC scheme, the scheme without trajectory optimization fails to obtain the performance gain brought by the fact that the UAV can optimize its trajectory to improve the channel condition between the UAV and users or the BS. (ii) The superior performance improvement of the suggested MEC scheme over the conventional RIS-assisted scheme is attributed to the enhanced regulatory capabilities of the STAR-RIS. Unlike the traditional RIS, the STAR-RIS can effectively modify the phases and amplitudes of the incident signals, thus leading to a more flexible and efficient operation. This also presents a huge application potential of the STAR-RIS in wireless communication systems. (iii) The MEC scheme employing uniform time slot partition demonstrates the least improvement in performance when contrasted with other MEC schemes, since this time scheduling will result in users experiencing high channel quality being unable to be allocated additional time for task offloading, indicating the importance of the reasonable time allocation. (iv) The uniform energy division structure constrains the modulation capabilities of the STAR-RIS, preventing it from effectively allocating signal energy according to the transmission conditions. (v) The MRT scheme designs the active beamforming variables by maximizing the energy of the desired signal but overlooks the interference among users. In contrast, the proposed scheme comprehensively considers both enhancing the desired signal's energy and suppressing interference among users.

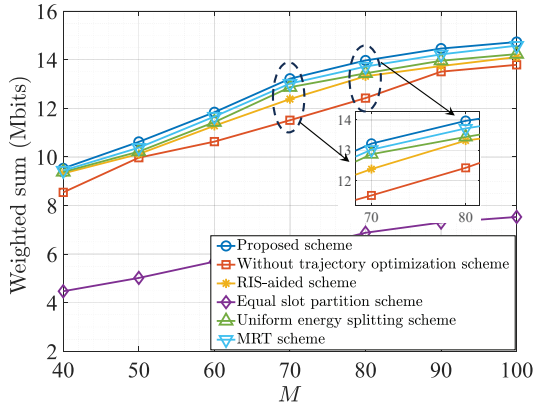

Fig. 5. Weight sum between l^{o}_{min} and l^{c}_{min} versus the number of elements equipped at the STAR-RIS with $N = 50$, $N_t = 6$, $L_o = 5$ Mbits, $L_c = 2$ Mbits and $\omega_o = \omega_c$ =0.5.

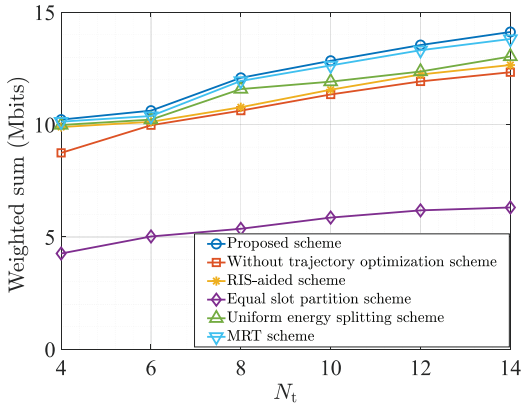

Fig. 6. Weight sum between l^{o}_{min} and l^{c}_{min} versus the number of antennas N_t with $M = 50$, $N = 50$, $L_o = 5$ Mbits, $L_c = 2$ Mbits and $\omega_o = \omega_c = 0.5$.

Then, we investigate the influence of the number of antennas, i.e., N_t, on the weighted sum of the minimum computational task and minimum communication data among users

taking into amount $M = 50$, $N = 50$, $L_{\rm o} = 5$ Mbits, $L_{\rm c} = 2$ Mbits and $\omega_{\rm o} = \omega_{\rm c} = 0.5$, as shown in Fig. 6. Specifically, it is observed that the performance of all schemes improves as the value of $N_{\rm t}$ rises, although the overall effect on performance gain is modest. The rationale behind this phenomenon lies in the observation that augmenting the quantity of antennas yields only a limited enhancement in the spatial multiplexing degrees of freedom. Similarly, the suggested MEC scheme continues to demonstrate the most significant performance improvement, whereas the equal time slot partition scheme shows the least improvement, falling short of half the performance gain attained by the proposed scheme. It is worth noting that there is a growing performance gap between the traditional RIS-aided scheme and the proposed scheme as the number of antennas increases, which further demonstrates the superiority of the STAR-RIS in assisting the STOC. Furthermore, the uniform energy splitting scheme shows a slight performance advantage over the traditional RIS-aided scheme, indicating the significance of simultaneously transmitting and reflecting phase design for each element.

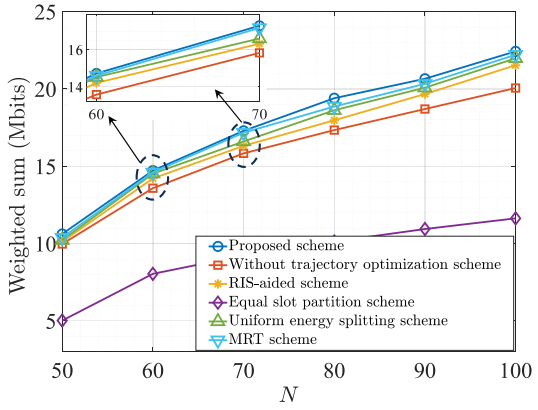

Fig. 7. Weight sum between $l^{\rm o}_{\rm min}$ and $l^{\rm c}_{\rm min}$ versus the number of time slot N with $M = 50$, $N_{\rm t} = 6$, $L_{\rm o} = 5$ Mbits, $L_{\rm c} = 2$ Mbits, and $\omega_{\rm o} = \omega_{\rm c} = 0.5$.

The impact of the quantity of time slots on the weighted sum between $l^{\rm o}_{\rm min}$ and $l^{\rm c}_{\rm min}$ is investigated in Fig. 7 using the specified parameters: $M = 50$, $N_{\rm t} = 6$, $L_{\rm o} = 5$ Mbits, $L_{\rm c} = 2$ Mbits, and $\omega_{\rm o} = \omega_{\rm c} = 0.5$. Similarly, as the value of N increases, all schemes demonstrate a consistent rise with a diminished rate of growth, which is because users are allocated more time to offload their tasks and transmit their information to the BS. Furthermore, the proposed scheme achieves the highest performance gain, while the scheme with the equal time slot partition still provides the lowest performance gain for the considered MEC network. Note that there is an increasing disparity in performance between the suggested scheme and the scheme lacking trajectory optimization, which is due to the fact that the UAV has more sufficient time to refine its position, ensuring a superior channel connection with users or the BS. As a result, the computational and communication capabilities of the MEC system will experience enhancement.

The investigation in Fig. 8 explores the correlation between $L^{\rm o}_{\rm min}$ and $L_{\rm c}$ under the parameters $M = 50$, $N = 70$, $N_{\rm t} = 6$, $L_{\rm o} = 1$ Mbits, and $\omega_{\rm o} = \omega_{\rm c} = 0.5$. It is observed that the

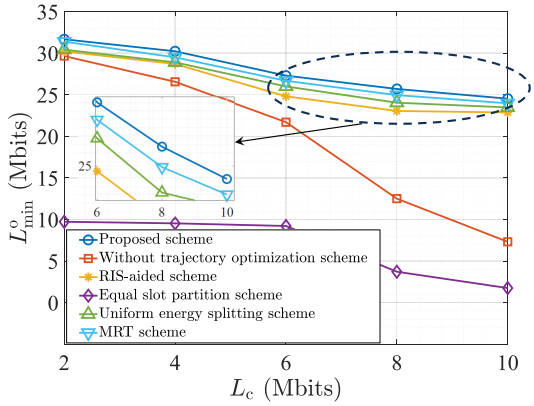

Fig. 8. The minimum computing data $L^{\rm o}_{\rm min}$ versus the minimum communication requirement $L_{\rm c}$ with $M = 50$, $N = 70$, $N_{\rm t} = 6$, $L_{\rm o} = 1$ Mbits and $\omega_{\rm o} = \omega_{\rm c} = 0.5$.

computational capacity of the MEC system under consideration is declining as the demand from users for communication services continues to rise for all MEC schemes. Specifically, the computational capabilities of the proposed scheme, the RIS-aided scheme, the uniform energy splitting scheme and MRT scheme all show a gradual decline as $L_{\rm c}$ increases, in contrast to the scheme without UAV trajectory optimization and equal time slot partition scheme, which both demonstrate a steep decrease. This result indicates that the optimization of the UAV trajectory and the reasonable time allocation play the critical roles in enhancing trade-off ability between the computation-oriented service and the communication-oriented service. Similarly, The performance improvement achieved through the proposed MEC scheme surpasses that of the other five baseline schemes.

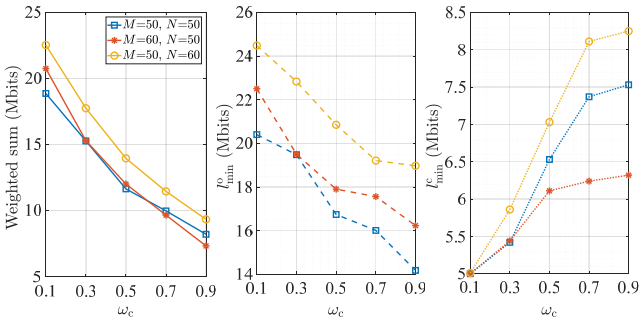

Fig. 9. Objective function, $l^{\rm o}_{\rm min}$ and $l^{\rm c}_{\rm min}$ versus weight factor $\omega_{\rm c}$ with $L_{\rm o} = 10$ Mbits, $L_{\rm c} = 5$ Mbits, and different number of elements deployed at the STAR-RIS, i.e., M and the time slots, i.e., N.

Fig. 9 illustrates the varied correlation of the weighted sum of $l^{\rm o}_{\rm min}$ and $l^{\rm c}_{\rm min}$, the minimum amount of the computing data, i.e., $l^{\rm o}_{\rm min}$, as well as the minimum amount of the communicational data, i.e., $l^{\rm c}_{\rm min}$ with the weight factor $\omega_{\rm c}$ considering different M and N. Specifically, the simulation results indicate a notable reduction in the minimum computational task for users as the weight factor linked to communication-oriented services increases in the analysed scenarios, whereas $l^{\rm min}_{\rm c}$ demonstrates an ascending trend. This phenomenon is coordinated with the fact that the signals of the tasks offloading and the signals of the transmitting message share the same

spectral resources in the considered system. Consequently, as the priority of communication-oriented services elevates, the system will intensify its focus on improving users' communication services and reduce the computational ability of the system. Furthermore, while $l_{\min}^{\mathrm{o}}$ and $l_{\min}^{\mathrm{c}}$ demonstrate opposing trends in relation to the increase of ω_{c}, the objective function undergoes a significant decline. The reason for this occurrence is due to the signals' dual-path loss experienced during information transmission before reaching the BS. Consequently, the potential for enhancing communication-focused services is severely restricted, and a modest slight progress may sacrifice more computing power.

V. Conclusion and Prospect

In this paper, we initially propose a novel MEC scheme supported by STAR-RIS and UAV, which takes account of the co-existence of the computation-oriented and communication-oriented services in networks. Specifically, thanks to its full-space modulation capability of the STAR-RIS, the horizontally mounted STAR-RIS allows users to simultaneously offload their computing tasks to the MEC servers situated at the BS and the UAV, which can effectively tackle the challenges faced by many exiting MEC schemes. Additionally, users requiring communication-oriented services in wireless networks can benefit from STAR-RIS's reflective modulation capability to enhance their communication experience. Unlike existing MEC schemes, the proposed approach simultaneously leverages the QoS requirements of both computation-oriented and communication-oriented services to comprehensively evaluate the performance of MEC networks, providing a feasible and realistic solution for implementing STOC in practical MEC networks. To evaluate the effectiveness of the proposed MEC scheme, an optimization problem is formulated with the objective of maximizing the weighted sum of the minimum computing data and the communication data among users, while ensuring the QoS constraints. To effectively address this non-convex problem, an iterative algorithm based on the SDR method and SCA technique is designed. The effectiveness for performance enhancement of the proposed MEC scheme and the developed optimization algorithm are assessed through numerical simulations in comparison with five benchmarks, including the traditional RIS-assisted scheme.

This paper provides an initial contribution to the field of aerial STAR-RIS-assisted MEC scheme for STOC. For future works, several pertinent potential use cases can be recognized: (i) **Industrial IoT applications**: The proposed aerial STAR-RIS-assisted MEC scheme enables efficient data offloading from numerous sensor nodes to edge servers for real-time processing, leveraging its bi-directional task offloading capability. (ii) **Disaster recovery and remote communication**: The aerial STAR-RIS model can enhance the network coverage, spectral efficiency, and system capacity in remote or disaster-affected areas, providing stable communications for rescue operations. (iii) **Multi-Service integration**: This work establishes a foundation for future communication networks supporting the coexistence of diverse services, offering scalable and practical solutions. Additionally, this study focuses on the energy splitting protocol of STAR-RIS, and single UAV system. It is meaningful to explore the mode selection and time switching protocols for STAR-RIS as well as multiple aerial STAR-RIS-supported communication scenarios in future. Furthermore, incorporating the sensing-oriented service into the proposed MEC scheme and considering more practical discrete phase-shifts are important topics for future investigations.

Appendix A
Proof of Theorem 1

Firstly, the Cholesky deposition is leveraged to depose $\mathbf{V}_{-k}$ as $\mathbf{V}_{-k}[n] = \mathbf{C}[n]\mathbf{C}^H[n]$, let $\tilde{\mathbf{w}}_k[n] = \mathbf{C}^H[n]\mathbf{w}_k[n]$. The equivalent optimization problem for (20) without constraint can be transformed as

$$\begin{aligned} \max_{\tilde{\mathbf{w}}_k[n]} \ & \tilde{\mathbf{w}}_k^H[n]\mathbf{C}^{-1}[n]\mathbf{V}_k[n]\mathbf{C}^{-H}[n]\tilde{\mathbf{w}}_k[n] \\ \text{s.t.} \ & \tilde{\mathbf{w}}_k^H[n]\tilde{\mathbf{w}}_k[n] = c, \end{aligned} \tag{49a}$$

where $c > 0$ is a constant.

Actually, this problem can be easily solved using the Lagrange multiplier. Specifically, the Lagrange function of the optimization problem (49) can be expressed as

$$\begin{aligned} \mathcal{L}(\tilde{\mathbf{w}}_k[n], \widehat{\lambda}) = & - \tilde{\mathbf{w}}_k^H[n]\mathbf{C}^{-1}[n]\mathbf{V}_k[n]\mathbf{C}^{-H}[n]\tilde{\mathbf{w}}_k[n] + \\ & \widehat{\lambda}(\tilde{\mathbf{w}}_k^H[n]\tilde{\mathbf{w}}_k[n] - c). \end{aligned} \tag{50}$$

The first-order partial derivative of $\mathcal{L}(\tilde{\mathbf{w}}_k[n], \widehat{\lambda})$ w.r.t. $\tilde{\mathbf{w}}_k[n]$ and $\widehat{\lambda}$ can be respectively derived as

- $\frac{\partial \mathcal{L}}{\partial \tilde{\mathbf{w}}_k[n]} = -2\mathbf{C}^{-1}[n]\mathbf{V}_k[n]\mathbf{C}^{-H}[n]\tilde{\mathbf{w}}_k[n] + 2\widehat{\lambda}\tilde{\mathbf{w}}_k[n]$,
- $\frac{\partial \mathcal{L}}{\partial \widehat{\lambda}} = \tilde{\mathbf{w}}_k^H[n]\tilde{\mathbf{w}}_k[n] - c$.

Let $\frac{\partial \mathcal{L}}{\partial \tilde{\mathbf{w}}_k[n]} = 0$ and $\frac{\partial \mathcal{L}}{\partial \widehat{\lambda}} = 0$, the optimal $\tilde{\mathbf{w}}_k[n]$ should satisfies

$$\begin{cases} \mathbf{C}^{-1}[n]\mathbf{V}_k[n]\mathbf{C}^{-H}[n]\tilde{\mathbf{w}}_k[n] = \widehat{\lambda}\tilde{\mathbf{w}}_k[n], \\ \tilde{\mathbf{w}}_k^H[n]\tilde{\mathbf{w}}_k[n] = c. \end{cases} \tag{51}$$

Based on the the result presented in (51), we can find that the optimal $\tilde{\mathbf{w}}_k[n]$ is the eigenvector corresponding to the eigenvalue $\widehat{\lambda}$ of the matrix $\mathbf{C}^{-1}[n]\mathbf{V}_k[n]\mathbf{C}^{-H}[n]$. Therefore, in order to maximize the objective function of the optimization problem (49), the optimal $\tilde{\mathbf{w}}_k[n]$ is constrained to the eigenvector associated with the maximum eigenvalue of the matrix $\mathbf{C}^{-1}[n]\mathbf{V}_k[n]\mathbf{C}^{-H}[n]$, denoted as $\tilde{\mathbf{w}}_k^{\mathrm{opt}}[n] = \mathrm{eigvector}\left\{ \max\left\{ \mathrm{eig}\left\{\mathbf{C}^{-1}[n]\mathbf{V}_k[n]\mathbf{C}^{-H}[n]\right\}\right\}\right\}$. Thus, the optimal $\mathbf{w}_k[n]$ can be derived as

$$\mathbf{w}_k^{\mathrm{opt}}[n] = \frac{\mathbf{C}^{-H}[n]\tilde{\mathbf{w}}_k^{\mathrm{opt}}[n]}{\left\|\mathbf{C}^{-H}[n]\tilde{\mathbf{w}}_k^{\mathrm{opt}}[n]\right\|}. \tag{52}$$

References

[1] Y. Mao, C. You, J. Zhang, K. Huang, and K. B. Letaief, "A survey on mobile edge computing: The communication perspective," *IEEE Commun. Surveys & Tuts.*, vol. 19, no. 4, pp. 2322–2358, 2017.

[2] M. Othman, S. A. Madani, S. U. Khan *et al.*, "A survey of mobile cloud computing application models," *IEEE Commun. Surveys & Tuts.*, vol. 16, no. 1, pp. 393–413, 2013.

[3] X. Hu, K.-K. Wong, and K. Yang, "Wireless powered cooperation-assisted mobile edge computing," *IEEE Trans. Wireless Commun.*, vol. 17, no. 4, pp. 2375–2388, 2018.

[4] X. Chen, "Decentralized computation offloading game for mobile cloud computing," *IEEE Trans. Parallel Distrib. Syst.*, vol. 26, no. 4, pp. 974–983, 2014.

[5] S. Bi and Y. J. Zhang, "Computation rate maximization for wireless powered mobile-edge computing with binary computation offloading," *IEEE Trans. Wireless Commun.*, vol. 17, no. 6, pp. 4177–4190, 2018.

[6] J. Bi, H. Yuan, S. Duanmu, M. Zhou, and A. Abusorrah, "Energy-optimized partial computation offloading in mobile-edge computing with genetic simulated-annealing-based particle swarm optimization," *IEEE Internet Things J.*, vol. 8, no. 5, pp. 3774–3785, 2020.

[7] C.-L. Chen, C. G. Brinton, and V. Aggarwal, "Latency minimization for mobile edge computing networks," *IEEE Trans. Mobile Comput.*, vol. 22, no. 4, pp. 2233–2247, 2021.

[8] G. Cui, X. Li, L. Xu, and W. Wang, "Latency and energy optimization for MEC enhanced SAT-IoT networks," *IEEE Access*, vol. 8, pp. 55 915–55 926, 2020.

[9] S. Jeong, O. Simeone, and J. Kang, "Mobile edge computing via a UAV-mounted cloudlet: Optimization of bit allocation and path planning," *IEEE Trans. Veh. Technol.*, vol. 67, no. 3, pp. 2049–2063, 2017.

[10] M. Li, N. Cheng, J. Gao, Y. Wang, L. Zhao, and X. Shen, "Energy-efficient UAV-assisted mobile edge computing: Resource allocation and trajectory optimization," *IEEE Trans. Veh. Technol.*, vol. 69, no. 3, pp. 3424–3438, 2020.

[11] X. Hu, K.-K. Wong, K. Yang, and Z. Zheng, "UAV-assisted relaying and edge computing: Scheduling and trajectory optimization," *IEEE Trans. Wireless Commun.*, vol. 18, no. 10, pp. 4738–4752, 2019.

[12] X. Hu, K.-K. Wong, and Y. Zhang, "Wireless-powered edge computing with cooperative UAV: Task, time scheduling and trajectory design," *IEEE Trans. Wireless Commun.*, vol. 19, no. 12, pp. 8083–8098, 2020.

[13] T. Zhang, Y. Xu, J. Loo, D. Yang, and L. Xiao, "Joint computation and communication design for UAV-assisted mobile edge computing in IoT," *IEEE Trans. Ind. Inform.*, vol. 16, no. 8, pp. 5505–5516, 2019.

[14] Y. Xu, T. Zhang, Y. Liu, D. Yang, L. Xiao, and M. Tao, "UAV-assisted MEC networks with aerial and ground cooperation," *IEEE Trans. Wireless Commun.*, vol. 20, no. 12, pp. 7712–7727, 2021.

[15] X. Hu, K.-K. Wong, C. Masouros, and S. Jin, "IRS-Aided Mobile Edge Computing: From Optimization to Learning," *Intelligent Surfaces Empowered 6G Wireless Network*, pp. 207–228, 2023.

[16] X. Qin, Z. Song, T. Hou, W. Yu, J. Wang, and X. Sun, "Joint optimization of resource allocation, phase shift and UAV trajectory for energy-efficient RIS-assisted UAV-enabled MEC systems," *IEEE Trans. Green Commun. Netw.*, 2023.

[17] H. Mei, K. Yang, J. Shen, and Q. Liu, "Joint Trajectory-Task-Cache Optimization With Phase-Shift Design of RIS-Assisted UAV for MEC," *IEEE Wireless Commun. Lett.*, vol. 10, no. 7, pp. 1586–1590, 2021.

[18] Y. Xu, T. Zhang, Y. Liu, D. Yang, L. Xiao, and M. Tao, "Computation capacity enhancement by joint UAV and RIS design in IoT," *IEEE Internet Things J.*, vol. 9, no. 20, pp. 20 590–20 603, 2022.

[19] H. Hu, Z. Sheng, A. A. Nasir, H. Yu, and Y. Fang, "Computation Capacity Maximization for UAV and RIS Cooperative MEC System With NOMA," *IEEE Commun. Lett.*, vol. 28, no. 3, pp. 592–596, 2024.

[20] Z. Zhai, X. Dai, B. Duo, X. Wang, and X. Yuan, "Energy-efficient UAV-mounted RIS assisted mobile edge computing," *IEEE Wireless Commun. Lett.*, vol. 11, no. 12, pp. 2507–2511, 2022.

[21] B. Duo, M. He, Q. Wu, and Z. Zhang, "Joint dual-UAV trajectory and RIS design for ARIS-assisted aerial computing in IoT," *IEEE Internet Things J.*, 2023.

[22] X. Mu, Y. Liu, L. Guo, J. Lin, and R. Schober, "Simultaneously tansmitting and reflecting (STAR) RIS aided wireless communications," *IEEE Trans. Wireless Commun.*, vol. 21, no. 5, pp. 3083–3098, 2022.

[23] Y. Liu, X. Mu, J. Xu, R. Schober, Y. Hao, H. V. Poor, and L. Hanzo, "STAR: Simultaneous transmission and reflection for 360° coverage by intelligent surfaces," *IEEE Wireless Commun.*, vol. 28, no. 6, pp. 102–109, 2021.

[24] H. Xiao, X. Hu, P. Mu, W. Wang, T.-X. Zheng, K.-K. Wong, and K. Yang, "Simultaneously Transmitting and Reflecting RIS (STAR-RIS) Assisted Multi-Antenna Covert Communication: Analysis and Optimization," *IEEE Trans. Wireless Commun.*, pp. 1–1, 2023.

[25] H. Xiao, X. Hu, A. Li, W. Wang, Z. Su, K.-K. Wong, and K. Yang, "STAR-RIS Enhanced Joint Physical Layer Security and Covert Communications for Multi-antenna mmWave Systems," *IEEE Trans. Wireless Commun.*, pp. 1–1, 2024.

[26] H. Xiao, X. Hu, T.-X. Zheng, and K.-K. Wong, "STAR-RIS Assisted Covert Communications in NOMA Systems," *IEEE Trans. Veh. Technol.*, vol. 73, no. 4, pp. 5941–5946, 2024.

[27] Z. Liu, X. Li, H. Ji, H. Zhang, and V. C. Leung, "Toward STAR-RIS-Empowered Integrated Sensing and Communications: Joint Active and Passive Beamforming Design," *IEEE Trans. Veh. Technol.*, 2023.

[28] Y. Wang, Z. Yang, J. Cui, P. Xu, G. Chen, T. Q. Quek, and R. Tafazolli, "Optimizing the Fairness of STAR-RIS and NOMA Assisted Integrated Sensing and Communication Systems," *IEEE Trans. Wireless Commun.*, 2023.

[29] N. Xue, X. Mu, Y. Liu, and Y. Chen, "NOMA Assisted Full Space STAR-RIS-ISAC," *IEEE Trans. Wireless Commun.*, pp. 1–1, 2024.

[30] X. Qin, Z. Song, T. Hou, W. Yu, J. Wang, and X. Sun, "Joint resource allocation and configuration design for STAR-RIS-enhanced wireless-powered MEC," *IEEE Trans. Commun.*, vol. 71, no. 4, pp. 2381–2395, 2023.

[31] Z. Liu, Z. Li, M. Wen, Y. Gong, and Y.-C. Wu, "STAR-RIS-aided mobile edge computing: Computation rate maximization with binary amplitude coefficients," *IEEE Trans. Commun.*, 2023.

[32] P. S. Aung, L. X. Nguyen, Y. K. Tun, Z. Han, and C. S. Hong, "Aerial STAR-RIS Empowered MEC: A DRL Approach for Energy Minimization," *IEEE Wireless Commun. Lett.*, 2024.

[33] H. Zhang, N. Shlezinger, F. Guidi, D. Dardari, M. F. Imani, and Y. C. Eldar, "Beam focusing for near-field multiuser MIMO communications," *IEEE Trans. Wireless Commun.*, vol. 21, no. 9, pp. 7476–7490, 2022.

[34] R. A. Horn and C. R. Johnson, *Matrix analysis*. Cambridge Univ. Press, 2012.

[35] Z.-Q. Luo, W.-K. Ma, A. M.-C. So, Y. Ye, and S. Zhang, "Semidefinite relaxation of quadratic optimization problems," *IEEE Signal Process. Mag.*, vol. 27, no. 3, pp. 20–34, 2010.

Han Xiao received the M.Eng. degree in Vehicle Engineering from Dalian University of Technology, Dalian, China, in 2021. He is currently pursuing a Ph.D. degree at the School of Information and Communications Engineering, Xi'an Jiaotong University, Xi'an, China. His research interests include physical layer security, covert communications, mobile edge computing and reconfigurable intelligent surface.

Xiaoyan Hu (Member, IEEE) received the Ph.D. degree in Electronic and Electrical Engineering from University College London (UCL), London, U.K., in 2020. From 2019 to 2021, she was a Research Fellow with the Department of Electronic and Electrical Engineering, UCL, U.K. She is currently an Associate Professor with the School of Information and Communications Engineering, Xi'an Jiaotong University, Xi'an, China. Her research interests are in the areas of 5G&6G wireless communications, including topics such as edge computing, reconfigurable intelligent surface, UAV communications, integrated sensing and communications (ISAC), secure&covert communications, and learning-based communications. She is the recipient of the IEEE Communication Society Big Data 2023 Best Influential Journal Paper Award. She has been recognized as an Exemplary Reviewer for IEEE COMMUNICATIONS LETTERS. From 2020 to 2023, she served as the Assistant to the Editor-in-Chief of IEEE WIRELESS COMMUNICATIONS LETTERS, and she is currently serving as an Associate Editor for IEEE WIRELESS COMMUNICATIONS LETTERS. She has also served as a Guest Editor for ELECTRONICS on Physical Layer Security and for CHINA COMMUNICATIONS Blue Ocean Forum on MAC and Networks.

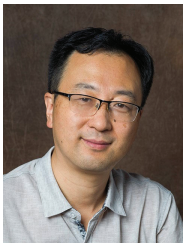

Wenjie Wang (Senior Member, IEEE) received the B.S., M.S., and Ph.D. degrees in Information and Communications Engineering from Xi'an Jiaotong University, Xi'an, China, in 1993, 1998, and 2001, respectively. He was a Visiting Scholar with the Department of Electrical and Computer Engineering, University of Delaware, Newark, DE, USA, from 2009 to 2010. Now, he is a Professor and the Dean of the School of Information and Communications Engineering, Xi'an Jiaotong University. His research interests include ad-hoc networks, smart antennas, wireless communication, signal processing, artificial intelligence, and data analysis.

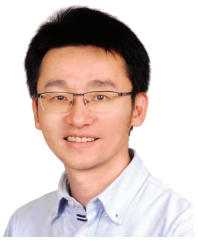

Zhou Su (Senior Member, IEEE) has published technical papers, including top journals and top conferences, such as IEEE JOURNAL ON SELECTED AREAS IN COMMUNICATIONS, IEEE TRANSACTIONS ON INFORMATION FORENSICS AND SECURITY, IEEE TRANSACTIONS ON DEPENDABLE AND SECURE COMPUTING, IEEE TRANSACTIONS ON MOBILE COMPUTING, IEEE/ACM TRANSACTION ON NETWORKING, and INFOCOM. His research interests include multimedia communication, wireless communication, and network traffic. He received the Best Paper Award of International Conference IEEE ICC2020, IEEE BigdataSE2019, and IEEE CyberSciTech2017. He is also an Associate Editor of IEEE INTERNET OF THINGS JOURNAL, IEEE OPEN JOURNAL OF THE COMPUTER SOCIETY, and *IET Communications*.

Kai-Kit Wong (Fellow, IEEE) received the BEng, the MPhil, and the PhD degrees, all in Electrical and Electronic Engineering, from the Hong Kong University of Science and Technology, Hong Kong, in 1996, 1998, and 2001, respectively. After graduation, he took up academic and research positions at the University of Hong Kong, Lucent Technologies, Bell-Labs, Holmdel, the Smart Antennas Research Group of Stanford University, and the University of Hull, UK. He is currently the Chair of Wireless Communications with the Department of Electronic and Electrical Engineering, University College London, UK. His current research centers around 5G and beyond mobile communications, including topics such as massive MIMO, full-duplex communications, millimetre-wave communications, edge caching and fog networking, physical layer security, wireless power transfer and mobile computing, V2X communications, fluid antenna communications systems, and of course cognitive radios. He is a co-recipient of the 2013 IEEE Signal Processing Letters Best Paper Award and the 2000 IEEE VTS Japan Chapter Award at the IEEE Vehicular Technology Conference in Japan in 2000, and a few other international best paper awards. He is Fellow of IEEE and IET and is also on the editorial board of several international journals. He has served as Senior Editor for IEEE COMMUNICATIONS LETTERS since 2012 and for IEEE WIRELESS COMMUNICATIONS LETTERS since 2016. He had also previously served as Associate Editor for IEEE SIGNAL PROCESSING LETTERS from 2009 to 2012 and Editor for IEEE TRANSACTIONS ON WIRELESS COMMUNICATIONS from 2005 to 2011. He was also Guest Editor for IEEE JSAC SI on virtual MIMO in 2013 and on physical layer security for 5G in 2018. He has been the Editor-in-Chief of the IEEE WIRELESS COMMUNICATIONS LETTERS, since 2020.

Kun Yang (Fellow, IEEE) received his PhD from the Department of Electronic & Electrical Engineering of University College London (UCL), UK. He is currently a Chair Professor of University of Essex, UK and Nanjing University. His main research interests include wireless networks and communications, communication-computing cooperation, and new AI (artificial intelligence) for wireless. He has published 500+ papers and filed 50 patents. He serves on the editorial boards of a number of IEEE journals (e.g., IEEE WCM, TVT, TNB). He is a Deputy Editor-in-Chief of IET Smart Cities Journal. He has been a Judge of GSMA GLOMO Award at World Mobile Congress-Barcelona since 2019. He was a Distinguished Lecturer of IEEE ComSoc (2020-2021), a Recipient of the 2024 IET Achievement Medals and the Recipient of 2024 IEEE CommSoft TCs Technical Achievement Award. He is a Member of Academia Europaea (MAE), a Fellow of IEEE, a Fellow of IET and a Distinguished Member of ACM.